

1 **TITLE**

2 **Distinct immunological signatures discriminate severe COVID-19 from non-SARS-CoV-**  
3 **2-driven critical pneumonia**

4 **AUTHORS**

5 Stefanie Kreutmair<sup>1,2</sup>, Susanne Unger<sup>1,3</sup>, Nicolás Gonzalo Núñez<sup>1,3</sup>, Florian Ingelfinger<sup>1,3</sup>,  
6 Chiara Alberti<sup>1</sup>, Donatella De Feo<sup>1</sup>, Sinduya Krishnarajah<sup>1</sup>, Manuel Kauffmann<sup>1</sup>, Ekaterina  
7 Friebel<sup>1</sup>, Sepideh Babaei<sup>4</sup>, Benjamin Gaborit<sup>5</sup>, Mirjam Lutz<sup>1</sup>, Nicole Puertas Jurado<sup>1</sup>, Nisar P.  
8 Malek<sup>4</sup>, Siri Goepel<sup>4,6</sup>, Peter Rosenberger<sup>7</sup>, Helene A. Häberle<sup>7</sup>, Ikram Ayoub<sup>8</sup>, Sally Al-Hajj<sup>8</sup>,  
9 Jakob Nilsson<sup>9</sup>, Manfred Classen<sup>4,11</sup>, Roland Liblau<sup>10,11</sup>, Guillaume Martin-Blondel<sup>8,10,11</sup>,  
10 Michael Bitzer<sup>4,11</sup>, Antoine Roquilly<sup>5,11</sup>, Burkhard Becher<sup>1,11,12,\*</sup>

11 **AFFILIATIONS**

12 1 Institute of Experimental Immunology, University of Zurich, 5057 Zurich, Switzerland

13 2 German Cancer Consortium (DKTK) and German Cancer Research Center (DKFZ),  
14 Heidelberg, Partner Site Freiburg, 79106 Freiburg, Germany

15 3 These authors contributed equally

16 4 Department Internal Medicine I, Eberhard-Karls University, 72076 Tuebingen, Germany

17 5 Université de Nantes, CHU Nantes, Pôle anesthésie réanimations, Service d'Anesthésie  
18 Réanimation chirurgicale, Hôtel Dieu, 44093 Nantes, France

19 6 German Centre for Infection Research (DZIF), Partner Site Tuebingen, 72076 Tuebingen,  
20 Germany

21 7 Department of Anesthesiology and Intensive Care Medicine, Eberhard-Karls University,  
22 72076 Tuebingen, Germany

23 8 Centre de Physiopathologie Toulouse-Purpan, Université de Toulouse, Centre National de  
24 la Recherche Scientifique, Institut National de la Santé et de la Recherche Médicale, UPS,  
25 31024 Toulouse, France

26 9 Department of Immunology, University Hospital Zurich, 8006 Zurich, Switzerland

27 10 Department of infectious and tropical diseases, Toulouse University Hospital, 31059  
28 Toulouse, France

29 11 These authors contributed equally

30 12 Lead contact

## **HIGHLIGHTS**

GM-CSF+ T cells are a hallmark of severe respiratory syndrome independent of pathogen

T cell exhaustion and impaired early antiviral response is unique in severe COVID-19

Circulating NKT cell frequencies serve as a predictive biomarker for severe COVID-19

HLA profile links COVID-19 immunopathology to impaired virus recognition

## **eTOC BLURB**

The pathogen-specific immune alterations in severe COVID-19 remain unknown. Using longitudinal, high-dimensional single-cell spectral cytometry and algorithm-guided comparison of COVID-19 vs. non-SARS-CoV-2-pneumonia patient samples, Kreutmair et al. identify T and NK cell immune signatures specific to SARS-CoV-2. They furthermore reveal NKT cell frequency as a predictive biomarker for COVID-19 outcome prediction and link impaired virus recognition to HLA genetics.

## **KEYWORDS**

COVID-19, SARS-CoV-2, high-dimensional single cell analysis, immune profiling, immunophenotyping, spectral flow cytometry, biomarker, Hospital-acquired pneumonia, Cytokines, GM-CSF, HLA typing, peptide binding strength

31 **CONTACT INFO**

32 \* Correspondence to: [becher@immunology.uzh.ch](mailto:becher@immunology.uzh.ch)

33 **SUMMARY**

34 Immune profiling of COVID-19 patients has identified numerous alterations in both innate and  
35 adaptive immunity. However, whether those changes are specific to SARS-CoV-2 or driven  
36 by a general inflammatory response shared across severely ill pneumonia patients remains  
37 unknown. Here, we compared the immune profile of severe COVID-19 with non-SARS-CoV-  
38 2 pneumonia ICU patients using longitudinal, high-dimensional single-cell spectral cytometry  
39 and algorithm-guided analysis. COVID-19 and non-SARS-CoV-2 pneumonia both showed  
40 increased emergency myelopoiesis and displayed features of adaptive immune paralysis.  
41 However, pathological immune signatures suggestive of T cell exhaustion were exclusive to  
42 COVID-19. The integration of single-cell profiling with a predicted binding capacity of SARS-  
43 CoV-2-peptides to the patients' HLA profile further linked the COVID-19 immunopathology to  
44 impaired virus recognition. Towards clinical translation, circulating NKT cell frequency was  
45 identified as a predictive biomarker for patient outcome. Our comparative immune map serves  
46 to delineate treatment strategies to interfere with the immunopathologic cascade exclusive to  
47 severe COVID-19.

## 48 INTRODUCTION

49 The coronavirus disease 2019 (COVID-19) pandemic has affected over 50 million people  
50 worldwide and resulted in more than 3 million deaths as of April 2021 (World Health  
51 Organization, 2020a). The causative agent is severe acute RS (RS) coronavirus 2 (SARS-  
52 CoV-2) (Lu et al., 2020). The majority of people infected with SARS-CoV-2 are either  
53 asymptomatic or develop mild and self-limiting symptoms of fever, cough and shortness of  
54 breath. However, approximately 8% of COVID-19 patients go on to experience the severe  
55 complications of pneumonia, respiratory failure and acute respiratory distress syndrome  
56 (ARDS), frequently requiring admission to the intensive care unit (ICU) and mechanical  
57 ventilation (Iype and Gulati, 2020; O'Driscoll et al., 2020). Despite some clinical similarities to  
58 other severe respiratory infections causing multi-organ failure, COVID-19 presents unique  
59 clinical challenges that we do not yet know how to overcome: at present, the in-ICU mortality  
60 rate remains at approximately 50% (Armstrong et al., 2020). Thus there is an urgent need to  
61 understand how mild and severe SARS-CoV-2 infection differ from each other, and how they  
62 are distinct from other causes of severe RS.

63 While the factors underpinning severe COVID-19 are not yet completely understood, evidence  
64 suggests that extreme respiratory distress in these patients is primarily mediated by  
65 immunopathology (Hadjadj et al., 2020; Merad and Martin, 2020). Multiple reports observe  
66 differences in the proportions of immune cell populations in the peripheral blood of COVID-19  
67 patients compared to healthy individuals; in particular a marked lymphopenia that is  
68 accompanied by changes to the lymphocyte activation and exhaustion phenotypes, some of  
69 which are partly associated with severity of the disease (Cao, 2020; Mathew et al., 2020; Su  
70 et al., 2020; Zheng et al., 2020). Alongside these cellular characteristics, a cytokine storm,  
71 defined by a massive increase in circulating levels of inflammatory cytokines including IL-6,  
72 GM-CSF and TNF, drives disease progression and the development of lung immunopathology  
73 (Bastard et al., 2020; Bonaventura et al., 2020; Hadjadj et al., 2020; Lucas et al., 2020; Poland  
74 et al., 2020; Del Valle et al., 2020; Zhang et al., 2020b). However, due to the lack of large well-  
75 controlled studies on the immune responses of hospitalized patients with non-COVID-19  
76 critical pneumonias, the extent to which these immune changes are COVID-19-specific or  
77 common to other life-threatening pathogen-induced pneumonias remains unclear. Identifying  
78 those immune phenotypes and processes underlying severe COVID-19 would represent an  
79 important step forward in the rational development of new and more effective ways of treating  
80 this uniquely-challenging disease.

81 Here, we compared immune profiles in longitudinally collected blood samples from mild and  
82 severe COVID-19 patients, alongside a cohort of critically-ill patients suffering from pneumonia  
83 triggered by non-SARS-CoV-2 pathogens, and HCs. This enabled us to identify immune

84 signatures specific to SARS-CoV-2 and those shared with other pathogen-associated severe  
85 RS. Whereas emergency myelopoiesis and adaptive immune paralysis are common features  
86 of RS, signs of T cell exhaustion and reduced cytotoxicity were exclusive to COVID-19. Lastly,  
87 the identification of circulating NKT frequencies as a predictive biomarker for patient outcome  
88 could immediately serve for early patient stratification and decision-making.

## 89 RESULTS

### 90 Study participants, sampling protocols and experimental approach

91 We recruited three cohorts of participants: 57 COVID-19 patients (150 samples) from three  
92 independent centers across Germany (Tuebingen) and France (Toulouse and Nantes).  
93 COVID-19 patients were categorized into six severity grades based on the World Health  
94 Organization's (WHO) ordinal scale (World Health Organization, 2020b), that subdivides mild  
95 (severity grade 1-3, COVID-19m) and severe (severity grade 4-6, COVID-19s) disease. The  
96 second cohort included 25 patients admitted to the ICU with non-SARS-CoV-2 pneumonia  
97 (Hospital-acquired pneumonia (HAP) next to the third cohort: 21 healthy controls (HCs) (Fig.  
98 1A). For the HAP cohort, all episodes of pneumonia were classified as severe and required  
99 invasive mechanical ventilation. Comprehensive demographic data was collected and is  
100 provided in the Figures S1A and Table S1A and S1B.

101 COVID-19 patients gave blood samples between days 0 and 96 after their hospital admission  
102 (Table S1C, except one patient assigned to severity grade 1), while HAP patients gave a single  
103 blood sample at 1-4 days post-diagnosis of pneumonia, and HCs also donated once. In case  
104 of COVID-19 patients, the time from infection to hospital admission is on average 6.4 days  
105 (Lauer et al., 2020; Li et al., 2020). In total, we collected 196 blood samples across all cohorts.  
106 Blood samples were processed for full blood counts and standard biochemistry at the clinical  
107 centers, with peripheral blood mononuclear cells (PBMCs) isolated and cryopreserved for later  
108 analysis (Fig. 1A, S1A).

109 The samples were subjected to high-parametric single cell spectral flow cytometry (Fig. 1A,  
110 S1A, Table S1A). We employed three overlapping antibody panels targeting a range of cell  
111 surface molecules including the SARS-CoV-2 receptor ACE-2 (Table S2A), and cytokines  
112 (after short-term stimulation, Tables S2B and S2C). This immunprofiling approach enabled us  
113 to assess: (1) the overall lymphocyte and myeloid composition of PBMCs; (2) the relative  
114 abundance of T cell subsets and their effector or memory status; (3) levels of B cell  
115 differentiation; (4) levels of Natural killer (NK) cell differentiation; (5) the relative abundance of  
116 monocyte and DC subsets; (6) signs of lymphocyte activation and exhaustion; (7) production  
117 of lymphocyte cytokines; and (8) production of myeloid cytokines. All samples were quality  
118 screened (for details see Material and Methods) leading to the inclusion of 167 PBMC samples  
119 across all cohorts. Using computational data integration based on 50 markers from the  
120 spectral flow cytometry together with 25 clinical measures (e.g. age, sex, Body mass index  
121 (BMI), etc.) as well as HLA typing to ultimately define the severe COVID-19-specific immune  
122 landscape (Table S1A).

123 **Immunomonitoring reveals differing immune landscapes in COVID-19m, COVID-19s**  
124 **and HAP patients**

125 To generate an overview of the circulating immune compartment in COVID-19m and COVID-  
126 19s patients, we analyzed spectral flow cytometry data using FlowSOM-based clustering (Van  
127 Gassen et al., 2015) combined with UMAP dimensionality reduction (McInnes L Saul  
128 N, Großberger L, 2018) (Fig. 1B, S1B, S1C). Comparison of PBMCs from HCs and COVID-  
129 19 patients revealed numerous frequency alterations of canonical immune subsets among  
130 CD45<sup>+</sup> cells, except CD4<sup>+</sup> lymphocytes, NK cells and monocytes which were comparable  
131 across all time points (TPs) (Fig. S1D). Compared to COVID-19m, the severe disease was  
132 characterized by significantly lower frequencies of CD8<sup>+</sup> T cells, coupled with higher  
133 frequencies of B cells (Fig. S1D).

134 We next combined all cytometry parameters of the surface panel (Table S2A) to deeply  
135 phenotype T cell, B cell, NK cell, DC and monocyte subsets from each cohort, assessing their  
136 differentiation and activation state as well as their exhaustion profile. Following data integration  
137 and HAP inclusion, a principal component analysis (PCA) of the resulting immune landscapes  
138 showed a clear segregation of cells from HCs compared to both COVID-19 and HAP groups,  
139 while COVID-19s patients shared signatures both with COVID-19m and HAP patients (Fig.  
140 1C, S1E). Stratification of the COVID-19 cohort data by sex or age did not reveal marked  
141 differences in immune phenotypes (Fig. S1F, S1G).

142 To uncover the immunological dysregulation of COVID-19s that is distinct from the  
143 inflammatory, infectious immune signatures of HAP, we further enriched our dataset with an  
144 overall lymphoid and myeloid cytokine profile of the different subpopulations (Tables S2B and  
145 S2C). We introduced the statistical measure of the effect size (ES) to combine both  
146 significance and fold change in one single statistical value, as proposed for clinical trials before  
147 (McGough and Faraone, 2009; Sullivan and Feinn, 2012). We computed the ES of the Mann-  
148 Whitney U test between the analyzed groups (Fig. 1D). Applying the interpretation of ES by  
149 Cohen (0.1 - 0.3 small effect, >0.3 intermediate and large effect) (Cohen, 1977), we set the  
150 threshold for the comparison of mild versus severe COVID to 0.3. Due to the high number of  
151 features reaching the threshold of 0.3 in the comparison COVID-19s versus HAP, we applied  
152 a more stringent cut-off of 0.4 in order to exclusively filter COVID-19s-specific features. This  
153 revealed that mild and severe COVID-19 exhibit distinct immune signatures (represented by  
154 an ES > 0.3 and seen in the upper part of the dot plot in Fig. 1D), but in addition, COVID-19s  
155 and HAP could be distinguished by a set of immune features (displayed in the upper right  
156 square in Fig. 1D; threshold ES > 0.4 vs. HAP). Immune alterations in severe RS (COVID-19s  
157 and HAP) occurred within the T cell, NK cell, monocyte and DC compartments (Fig. 1E).

158 Taken together, COVID-19s presents immune features that are both shared and distinct from  
159 other pneumonia and affect all immune compartments except for B cells.

160 **Shared T cell features between severe pathogen-induced RSs highlight the emergence**  
161 **of hyperinflammatory and exhausted subsets in COVID-19s**

162 Following selection of the common immunological trajectories shared across severe RS  
163 patients (COVID-19s and HAP) (Fig. 1D, upper left square), we further extracted their dynamic  
164 manifestation in the COVID-19 cohort by correlation to disease severity and analysis over  
165 time. The identified patterns revealed predominantly the T cell compartment (Fig. 2A, 2B, S2A,  
166 S2B, Table S3). The reduction in CD4<sup>+</sup> CD8<sup>+</sup> (TCR $\gamma\delta$  enriched) T cell frequency appeared to  
167 be progressive, reaching its lowest during the second week of hospitalization (TP 3 (day 6-9))  
168 (Fig. 2C). Moreover, we observed significantly higher expression levels of PD-1 in COVID-19s  
169 patients already during the first 5 days of hospital admission, predominantly affecting the CD4<sup>+</sup>  
170 T cell compartment, pointing to a potential functional deficit in T helper (Th) cell immune  
171 responses (Fig. 2D). While in samples from COVID-19m patients PD-1 expression normalized  
172 at TP 5 (week 4-14), it remained elevated on memory CD4<sup>+</sup> T cell subsets in COVID-19s (Fig.  
173 S2C). In contrast to PD-1, the detected upregulation of the inhibitory receptor CTLA-4 on PMA  
174 and ionomycin-restimulated CD4<sup>+</sup> effector memory (EM) cells occurred only at later stages of  
175 disease (TP 3 and 4; day 6-15) (Fig. 2E, S2D). These findings point to a shared altered innate  
176 immune response and signs of hyperinflammation and exhaustion within the T cell  
177 compartment across all patients with severe RS.

178 In order to interrogate the cytokine polarization, the cells were briefly stimulated *in vitro* prior  
179 to spectral flow acquisition. The resulting cytokine profile of stimulated lymphoid  
180 subpopulations from COVID-19 patients showed significantly higher amounts of IL-21, as well  
181 as a shift towards a cytotoxic phenotype indicated by high levels of granzyme B and perforin  
182 in the T and NK cell compartments, relative to HCs (Fig. S2E, S2F, data not shown). CD107a  
183 on T and NK cells was similar in COVID-19s, COVID-19m and HCs (data not shown),  
184 suggesting not only equal cytotoxicity but also degranulation capacity across COVID-19  
185 disease severity. The same applies for TNF, IL-4, IL-6, and IL-17A, which failed to reach the  
186 cut-off of 0.3 ES when comparing mild and severe COVID-19 (Fig. 2F, S2G-J). However, we  
187 found increased production of interferon- $\gamma$  (IFN- $\gamma$ ), IL-2 and GM-CSF in COVID-19s.  
188 Specifically, higher frequencies of IFN- $\gamma$ -expressing CD8<sup>+</sup> EM, TEMRA (CCR7<sup>-</sup> CD45RA<sup>+</sup>) and  
189 TCR $\gamma\delta$  T cells (Fig. 2G) and IL-2-expressing TCR $\gamma\delta$  T cells were a common feature of severe  
190 RSs shared by COVID-19 and HAP (Fig. 2H). Elevated frequencies of GM-CSF-producing  
191 CD4<sup>+</sup> and CD8<sup>+</sup> TEMRA cells positively correlated with COVID-19 severity in the acute phase  
192 of disease (TP 1 and 2) (Fig. 2I, S2K, S2L). Single-cell RNA-seq analysis of blood cells from

193 COVID-19 patients - in absence of *ex vivo* stimulation - revealed strong expression of *CSF2*  
194 (encoding for GM-CSF) particularly in CD4<sup>+</sup> T cells (Fig. S2M). Detailed differentially  
195 expressed gene (DEG) analysis of *CSF2* high vs. low expressing CD4<sup>+</sup> T cells indicated these  
196 cells as a hyperinflammatory subset, strongly expressing *TNF*, *IL21*, *TNFRSF4*, *GPLY*,  
197 *CD40LG*, *CCL20*, *ICAM1* and demonstrating low *ANXA1* mRNA levels, among others (Fig.  
198 S2N).

199 Overall, these data demonstrate a T cell compartment marked by both hyperinflammatory and  
200 exhaustive features shared by patients with severe COVID-19 and non-SARS-CoV-2-induced  
201 RSs (HAP). Over time, this phenotype persists, particularly in disease courses of COVID-19s  
202 (Fig. 2J).

### 203 **Phenotypic alterations in innate immune signatures are shared in severe COVID-19 and** 204 **HAP**

205 We further characterized the identified DC and NK cell features shared by COVID-19s and  
206 HAP (Fig. 3A, Table S3). To reveal the dynamic changes over time, we displayed the COVID-  
207 19 cohorts together with HCs as baseline and HAP patients as comparison. Lower expression  
208 of HLA-DR in CD56<sup>low</sup> CD16<sup>-</sup> NK cells suggest a diminished cytotoxic response in COVID-19s  
209 (Fig. 3B-D, S3A) (Erokhina et al., 2020). Similarly, COVID-19s displayed reduced frequency  
210 of plasmacytoid DCs (pDC) (Fig. 3E-G, S3B). Although the pDC frequency was also different  
211 from HAP, the cut-offs of the ES were not reached. Upregulation of the Fas receptor CD95  
212 was detected in all DC subsets - particularly on pDCs - at early TPs 1 and 2 (Fig. S3C, S3D).  
213 This might play a role in the loss of those cells through Fas-mediated apoptosis.

214 To mimic SARS-CoV-2 infection *in vitro*, the PBMC samples were stimulated for 8h with the  
215 TLR7 and TLR8 agonist R848. In response, intermediate and non-classical monocytes as well  
216 as conventional DC2s (cDC2s) upregulated expression of the chemokine receptor CCR2 (Fig.  
217 S3E, S3F), but only the cDC2-related feature reached the cut-off for being COVID-19s-specific  
218 (>0.3 ES vs. COVID-19m) and positively correlated with the severity grade of SARS-CoV-2-  
219 mediated disease (Fig. 3H). As CCR2 expression on DCs is a hallmark of inflammation and  
220 required for their migration to the inflamed lung (Kvedaraite et al., 2020; Nakano et al., 2017),  
221 this could explain the invasion of DCs into the lungs of patients hospitalized with severe  
222 COVID-19. The NK and DC-specific dysregulation described here were already apparent  
223 during the early phase of the disease, and the vast majority of these changes persisted until  
224 TP 5 in severe COVID-19 patients, yet resolved in patients with COVID-19m (Fig. 3I). In line  
225 with reduced pDC frequencies, IFN- $\gamma$  levels in the serum of COVID-19s patients showed a  
226 robust trend towards reduction, when compared to COVID-19m (Fig. S3G).

227 To summarize, patients with severe RS show signs of diminished cytotoxicity combined with  
228 increased cell migration within the NK cell and DC compartment independent of the underlying  
229 pathogen.

### 230 **Impaired antigen-presentation distinguishes the immune response to SARS-CoV-2** 231 **versus other respiratory pathogens**

232 After defining several common immunological features characterizing the immune landscape  
233 of COVID-19s in common with HAP, we next extracted the features specific to SARS-CoV-2  
234 infection. We selected all immune traits characterizing COVID-19s (cut-off ES vs. COVID-19m  
235 > 0.3) and to further condense the signature uniquely existing in COVID-19s and being  
236 different from HAP, we set a strict cut-off ES 0.4 vs. HAP (Fig. 4A, Table S3). Building on the  
237 above-described common myeloid features, there were also phenotypic changes within this  
238 compartment that were specific to COVID-19s. Specifically, there was significantly lower  
239 expression of HLA-DR as well as the co-stimulatory ligand CD86 across antigen presenting  
240 cell (APC) subsets, which persisted throughout the duration of our study and were not shared  
241 to this extent by patients with mild COVID-19 disease (Fig. 4B, 4C, S4A, S4B). The protein  
242 expression of both HLA-DR and CD86 negatively correlated with the severity of COVID-19,  
243 with highest significance of this relationship within monocytes (Fig. 4D, 4E, S4C, S4D).  
244 Although the apparent paralysis in the APC compartment fulfilled the criteria for COVID-19s-  
245 specificity (Fig. 4F), this was largely driven by a more pronounced APC dysfunction in HAP,  
246 when compared to HCs (Fig. 4G, H). Taken together, the emerging overall picture of a myeloid  
247 compartment characterized by an impaired APC function – most likely due to emergency  
248 myelopoiesis - in COVID-19s. However, the data suggest that this is a feature shared across  
249 all patients with severe RS and not specific to the immune response against SARS-CoV-2.

### 250 **Distinct signatures of COVID-19s are exclusive to the lymphocyte compartment**

251 While most of the alterations in the monocyte and DC compartment were convergent in the  
252 two severe RSs, we identified COVID-19s-specific T and NK cell signatures (Fig. 5A, Table  
253 S3; ES COVID-19s vs. COVID-19m > 0.3 and vs. HAP > 0.4). A focused analysis of all T cell  
254 subsets (Fig. S5A) revealed a dramatic loss of NKT cells in COVID-19s as one of those  
255 signatures (Fig. 5B). This NKT cell reduction was already apparent within the first week after  
256 COVID-19-related hospital admission (TP 1 and 2). As shown in the Receiver Operating  
257 Characteristic (ROC) curve of Table S4, a cut-off for NKT frequency among T cells of 2.3%  
258 can distinguish severe COVID-19 patients from mild disease with a sensitivity of 100% already  
259 at day 0-2 after hospital admission. This finding defines NKT frequency as a powerful

260 predictive biomarker for COVID-19s evolution and furthermore suggesting a role of these cells  
261 in the first phase of disease.

262 In addition to the above-described upregulation of PD-1 predominantly in CD4<sup>+</sup> T cells, higher  
263 expression of PD-1 by CD4<sup>+</sup> EM cells turned out to be a feature unique to COVID-19s (ES vs  
264 HAP > 0.4), which positively correlated with severity grade (Fig. 5C, S5B). Chronically  
265 stimulated T cells overexpress inhibitory receptors including PD-1 and display poor effector  
266 capacity (Ahmadzadeh et al., 2009; Crawford et al., 2014; Huang et al., 2019a; Pauken and  
267 Wherry, 2015; Wu et al., 2014). By comparing *PDCD1* high and low expressing CD4<sup>+</sup> T cells  
268 using a single-cell RNA-seq dataset (Zhao et al., 2021), we found *PDCD1* high CD4<sup>+</sup> T cells  
269 to express genes associated with exhaustion (*HAVCR2*, *LAG3*, *CTLA4*, *TIGIT*, *BATF*) as well  
270 as reduced amounts of *TCF7*, *TNF*, *IL2RA*, *TNFRSF4*, *FAS*, *MIK167*, associated with T cell  
271 activation (Fig. S5C). This dataset supports the notion that the T cell compartment in COVID-  
272 19 patients is impaired or exhausted.

273 The protein expression of CD38, another activation marker, across several T cell subsets  
274 positively correlated with COVID-19 severity, with the highest significance ( $p < 0.0001$ ,  $R^2 =$   
275  $0.24$ ) in CD4<sup>-</sup> CD8<sup>-</sup> (TCR $\gamma\delta$  enriched) T cells (Fig. 5D, S5D). Furthermore, we observed a loss  
276 of the regulatory protein CD161 in CD4<sup>-</sup> CD8<sup>-</sup> (TCR $\gamma\delta$  enriched) T cells in COVID-19s (Fig.  
277 5E, S5E). This phenomenon is especially intriguing, as CD4<sup>-</sup> CD8<sup>-</sup> (TCR $\gamma\delta$  enriched) T cells  
278 share the transcriptional signatures of CD161-expressing Mucosa-Associated Invariant T  
279 (MAIT) cells, a CD8<sup>+</sup> T cell subset resembling innate-like sensors and mediators of antiviral  
280 responses (Fergusson et al., 2014, 2016).

281 Although failing to reach the stringent cut-off for being a unique COVID-19s specific feature  
282 (ES vs HAP > 0.4), CD161 was also expressed at a significantly lower level on immature and  
283 CD56<sup>low</sup> CD16<sup>+</sup> NK cells in the early phase of severe SARS-CoV-2 related illness compared  
284 to mild disease (Fig. S5F). Here, the kinetics of CD161 expression was low at the beginning  
285 of disease with a delayed hyperreactivity in COVID-19s (Fig. S5F). Further dissecting the NK  
286 cell compartment, CD95 expression in the CD56<sup>high</sup> NK subset positively correlated with  
287 severity of COVID-19 and represents a unique characteristic specific to SARS-CoV-2 infection  
288 (Fig. 5F, S5G). As in the DC compartment described before, the significant and specific  
289 reduction of this NK subset supports the Fas-mediated, activation-induced apoptosis as the  
290 mechanism underlying the shift from effector to immature NK cells (Fig. S5H).

291 Regarding the cytokine polarization profile, a reduced production of IFN- $\gamma$  in CD4<sup>+</sup> central  
292 memory (CM) T cells was found to be COVID-19s specific and reflects the loss of CD4<sup>+</sup>  
293 CXCR3<sup>+</sup> CCR6<sup>+</sup> (Th1 Th17-enriched) T cells (Fig. 5G, 5H). All features falling in the COVID-  
294 19s specific category and diverging from HAP recovered only partly, both in mild and severe

295 SARS-CoV-2 infected patients, pointing to a persisting dysfunctional T and NK cell  
296 compartment (Fig. 5I).

297 The recorded myeloid features in COVID-19s were even more pronounced in the HAP patients  
298 (Fig. 4G, 4H). In contrast, several identified COVID-19s specific T and NK cell features were  
299 clearly different from what has been observed in HC and HAP (Fig. 5B, 5E, 5H, 5J). Taken  
300 together, whereas changes in the myeloid compartment are shared across severe RS  
301 patients, our differential display approach extracted signatures of T cell exhaustion and altered  
302 early antiviral innate lymphoid response specific to the immune response to SARS-CoV-2.

### 303 **HLA profile links COVID-19 immunopathology to impaired virus recognition**

304 After defining the pathological immune landscape specific for SARS-CoV-2 and distinct from  
305 other pathogen-induced pneumonias, we next explored the degree of correlation existing  
306 across these and other COVID-19s-associated immune features in order to depict the overall  
307 immune network underlying COVID-19s. We therefore selected all signatures associated with  
308 COVID-19s (ES vs. COVID-19m > 0.3) from TP 1 and 2 and, for each feature, computed  
309 Pearson's r correlation values visualized in a heatmap plot for each COVID-19s and HAP (Fig.  
310 6A). Given the power of this multi-dimensional, global analysis tool, it was possible to identify  
311 correlation patterns within the immune network of the two investigated conditions, namely  
312 COVID-19s and HAP. Focusing on the interactive network underlying early and severe SARS-  
313 CoV-2 mediated disease, we discovered distinctive associations between different branches  
314 of adaptive and innate immunity, translating into correlation clusters between myeloid and T  
315 cells (#1), myeloid and NK cells (#2) as well as T and NK cells (#3) (Fig. 6A). These  
316 associations were weak in HAP, further supporting our claim of a SARS-CoV-2 specific  
317 immune landscape that characterizes severe disease courses.

318 Because of earlier evidence of SARS-CoV-2 peptide binding to Human Leukocyte Antigen  
319 (HLA) molecules differs across genotypes (Nguyen et al., 2020), we introduced next  
320 generation sequencing (NGS)-based HLA class I typing of 48 patients of our COVID-19 cohort.  
321 We calculated the predicted number of tightly binding (<50nm) SARS-CoV-2-derived peptides  
322 per HLA class I gene (based on every single underlying allele genotype) for each of our typed  
323 individuals (Fig. S6A, S6B, Table S5). This predicted binding capacity for HLA-A, HLA-B and  
324 HLA-C was further called HLA score 50. Next, we integrated this dataset to our single-cell  
325 immune profiling analysis and correlated this HLA-A, HLA-B and HLA-C score 50 to all our  
326 extracted severe COVID-19-associated immune features (Fig. 6B). This multi-omics approach  
327 allowed us to show that the majority of the severe COVID-19-associated immune features of  
328 the innate immune system (e.g. NKT frequency, HLA-DR in monocytes and DCs, etc.) was  
329 correlating with the SARS-CoV-2 binding strength (Fig. 6B). Meaning, that efficient HLA

330 binding capacity to SARS-CoV-2 peptides may mitigate the alterations of the innate immune  
331 system detected in COVID-19s. Also, the COVID-19s associated GM-CSF production in CD8<sup>+</sup>  
332 CM T cells positively correlated with high HLA scores. To conclude, the data suggests that  
333 weak HLA binding to SARS-CoV-2 peptides may at least in part drive the immunopathology  
334 in COVID-19.

335 To translate the complex immune signatures into clinical use, we correlated the COVID-19s-  
336 defining immune signatures with routine clinical parameters. In order to identify stratifying  
337 biomarkers in the very early phase of disease, we included features significantly associated  
338 with COVID-19s at TP 1 only. As every COVID-19 patient was graded according to the  
339 maximum severity of disease during the longitudinal follow-up of the study and this grading  
340 was allocated to every sample of the same patient, the included features of TP 1 fulfil the  
341 criteria to be predictive. Several blood values and BMI (indicated by an arrow) were highly  
342 correlated with our COVID-19s-defining immune signatures, thereby translating these  
343 immunological findings into clinical routine parameters (Fig. 6C). To further validate these  
344 promising candidates for outcome prediction, we linearly correlated them with COVID-19  
345 severity grade (Fig. 6D, S6C). Although the number of provided values was limited and several  
346 associations turned out to be significant but with a low R squared value, LDH and granulocyte  
347 counts showed a strong correlation with worsening of COVID-19, thus presenting easily  
348 applicable biomarkers (Fig. 6D, S6D).

349 In conclusion, we provide a translational path forward based on our differential immune map  
350 specific for severe SARS-CoV-2 infection combined with predicted HLA class I binding  
351 capacity to SARS-CoV-2 peptides, which can be used to guide therapeutic approaches aimed  
352 at interrupting the immunopathologic cascade of severe COVID-19.

### 353 **ACE2 expression in a CD4<sup>+</sup> T cell subset increases after *ex vivo* stimulation**

354 SARS-CoV-2 employs the angiotensin-converting enzyme 2 (ACE2) as its receptor for cellular  
355 entry (Prompetchara et al., 2020; Zhou et al., 2020). To determine potential entry sites within  
356 T cells we measured ACE2 expression across our immune map. We did not identify ACE2  
357 expression in steady state healthy T cell subpopulations, whereas samples from severe RS  
358 showed marginal expression, especially in the CD4<sup>+</sup> CXCR3<sup>+</sup> CCR6<sup>+</sup> (Th1 Th17-enriched)  
359 subset (Fig. 7A, 7B, 7C, S7A, S7B) which was significantly reduced in COVID-19s (Fig. 7D).  
360 When we profiled the stimulated PBMCs mimicking the COVID-19 inflammatory environment,  
361 we discovered a CD4<sup>+</sup> T cell subpopulation, of which approximately 75-80% expressed ACE2  
362 (Fig. 7E, 7F). This population emerged from samples of both healthy and COVID-19 patients  
363 and expressed CD25, PD-1 and CTLA4 (Fig. 7G, 7H, S7C). Further analysis of this subset  
364 demonstrated no relevant overlap with a specific cytokine polarization profile or FOXP3

365 expression (Fig. S7D, S7E). The presence of ACE2 expression on an activated CD4<sup>+</sup> T cell  
366 subset may provide a mechanism for virus entry and contribution to the immunopathological  
367 network of COVID-19.

368 **DISCUSSION**

369 The comparison of two cohorts of severe infectious RSs (COVID-19s and HAP) driven by  
370 different pathogens allowed us to uncover unique immune signatures in SARS-CoV-2  
371 mediated disease. Recent data describes the immunopathogenesis of HAP as critical illness-  
372 related immuno-suppression (Roquilly et al., 2019) mainly characterized by alterations in the  
373 IL-12 - IFN- $\gamma$  axis (Roquilly et al., 2017). Conversely, the COVID-19 immune response includes  
374 traits also occurring in other severe RS triggered by other pathogens such as influenza (Lee  
375 et al., 2020; Tian et al., 2020). However, mainly due to the small cohort sizes and lack of a  
376 comparable control group of patients suffering from non-SARS-CoV-2 driven severe RS, the  
377 COVID-19-specific immune signature remains elusive. Within our dataset already, a global  
378 PCA analysis of all immunophenotypes allowed for a clear separation between COVID-19s,  
379 COVID-19m, HAP and HCs. There was however a partial overlap between COVID-19s and  
380 HAP, revealing some core immune features associated with severe RS independent from the  
381 disease etiology.

382 Whilst previous studies described an impairment in the monocyte and DC compartment to be  
383 decisive for a severe COVID-19 course (Arunachalam et al., 2020; Kuri-Cervantes et al., 2020;  
384 Merad and Martin, 2020; Silvin et al., 2020), features which we confirmed here, those were  
385 found to not be exclusive to SARS-CoV-2-immunopathology. We confirmed loss of HLA-DR  
386 and CD86 expression in APCs, a finding associated with emergency myelopoiesis, where  
387 newly emerging myeloid cells show reduced APC capacity (Schulte-Schrepping et al., 2020).  
388 Recent data shows the secretion of CCL2 by airway macrophages and a concomitant  
389 upregulation of the CCL2-receptor CCR2 in peripheral blood monocytes of SARS-CoV-2  
390 infected patients; thus, extensive accumulation of monocytes and macrophages within  
391 alveolar spaces in COVID-19 lung autopsies suggests recruitment from circulation (Szabo et  
392 al., 2020). Our data support this, but in addition we observed that cDC2s also upregulated  
393 CCR2 expression with an even greater ES than monocytes. There is evidence for CCR2 being  
394 required for DC migration to the inflamed lung, respectively, while this is not the case in the  
395 steady state condition (Nakano et al., 2015, 2017). Thus, the declining number of cDC2s in  
396 the systemic circulation of COVID-19 patients may be a reflection of cDC2 extravasation into  
397 the affected lungs.

398 Alongside signatures shared in severe RS, we also extracted those specific to and unique in  
399 COVID-19s. These SARS-CoV-2-induced adaptations were restricted to the T and NK cell  
400 compartment. Several studies described an upregulation of PD-1 and CD38 alongside other  
401 activation and exhaustion markers, suggesting a hyperactivated and exhausted T cell  
402 compartment (De Biasi et al., 2020; Chen and Wherry, 2020). However, again, it was unclear  
403 as to whether this emerging pattern in lymphocytes is the result of severe RS in general, or is

404 specific to the immunopathology induced by SARS-CoV-2. We here describe an overall picture  
405 of T cell exhaustion and altered early antiviral innate lymphoid response unique to COVID-  
406 19s.

407 SARS-CoV-2 entry into the host cells is initiated by binding of the virus to the cell surface  
408 transmembrane receptor ACE2, which is predominantly expressed in epithelial cells of the  
409 lung, intestine and endothelial cells (Varga et al., 2020). Our analysis revealed the ability of  
410 highly activated CD4<sup>+</sup> T cells to express ACE2. Others also detected ACE2 positive  
411 lymphocytes in lungs COVID-19 patients (Ackermann et al., 2020; chen et al., 2020).  
412 Moreover, CD4<sup>+</sup> Th cell infection by SARS-CoV-2 occurs in an ACE2 dependent manner  
413 (Pierce et al., 2020; Pontelli et al., 2020). Compared to SARS-CoV, SARS-CoV-2 has a 10 -  
414 20-fold higher affinity for host membrane ACE2 (Wrapp et al., 2020). Thus, even low ACE2  
415 expression may be sufficient for viral entry. A direct infection of responding lymphocytes,  
416 leading to cell death and impaired SARS-CoV-2 clearance, goes in line with higher peripheral  
417 blood viral load positively correlating with COVID-19 severity (Han et al., 2020). In conclusion,  
418 the ability for SARS-CoV-2 to directly infect T cells provides yet another potential mechanism  
419 to describe the immunopathology of COVID-19.

420 The cytokine storm in COVID-19 is pronounced as one of the driving immunopathological  
421 features in SARS-CoV-2 mediated disease worsening (Merad and Martin, 2020; Moore and  
422 June, 2020; Del Valle et al., 2020). Our single-cell profiling of 11 cytokines did not result in  
423 higher frequencies of IL-6 and TNF (Del Valle et al., 2020), for which high plasma levels were  
424 described in COVID-19 patients, indicating neutrophils, monocytes and endothelial cells at the  
425 site of infection likely account for the dysregulated cytokine production. Nevertheless, we  
426 identified the cellular sources for GM-CSF as predominantly the CD4<sup>+</sup> and CD8<sup>+</sup> TEMRA  
427 subset - a feature of severe COVID-19 sharing with HAP - and documented correlation of the  
428 expression with COVID-19 severity. Our data complement two recent reports, which show that  
429 in particular lung invading T cells express GM-CSF (by using scRNA-seq) (Zhao et al., 2021)  
430 and that GM-CSF serum levels are elevated in COVID-19 patients (Thwaites et al., 2021).  
431 Supportive, elevated circulating GM-CSF<sup>+</sup> CD4<sup>+</sup> T cell levels are predictive of poor outcomes  
432 in sepsis patients (Huang et al., 2019b). Collectively, this suggests GM-CSF to be an early  
433 driver of the underlying immunopathological cascade in COVID-19s, thereby being a  
434 promising therapeutic target (NRI, GEM TRIAL, Clinical trial identifiers NCT04400929 and  
435 NCT04411680, (Bonaventura et al., 2020; Bosteels et al., 2020; Lang et al., 2020; De Luca et  
436 al., 2020)).

437 Using NGS-based HLA-typing and further integration of this dataset into our single-cell  
438 immune profiling analysis, this multi-omics approach provides deep insights into the COVID-  
439 19 immunopathology and a potential genetic influence: while COVID-19s-associated innate

440 immune alterations were less pronounced in patients with predicted high HLA class I binding  
441 capacity to SARS-CoV-2 peptides, GM-CSF production in CD8<sup>+</sup> CM T cells – a feature  
442 associated with severe COVID-19 disease - was increased. The occurrence of both mild and  
443 severe COVID-19-associated immune features in patients with strong SARS-CoV-2  
444 recognition (high HLA score 50) could further explain the inconsistent reports which attempt  
445 to link HLA class I binding capacity to SARS-CoV-2 peptides to COVID-19 severity (Ellinghaus  
446 et al., 2020; Iturrieta-Zuazo et al., 2020). By combining the single-cell immune mapping with  
447 HLA genetics, we uncovered a link between the HLA profile and impaired virus recognition in  
448 COVID-19.

449 Due to emerging follow-up studies, an increased number of COVID-19 patients are described  
450 to experience prolonged symptomatology. This phenomenon, referred to as "long COVID"  
451 affects around 10% of the cases. An attributed reason for long-lasting complaints is persistent  
452 tissue damage in severe cases. Nevertheless, patients following mild SARS-CoV-2 infections  
453 also suffer from prolonged symptoms (Iadecola et al., 2020; Mahase, 2020). We identified  
454 several immune features, predominantly of the T and NK compartment, which did not rebound  
455 at the end of our study, several weeks after infection. Thus, prolonged immune dysregulation,  
456 long after primary pathogen encounter, could play a role in "long COVID".

457 An additional aspect of our study was to identify predictive biomarkers of severe COVID-19  
458 patient outcomes. An earlier study identified the frequency of circulating MAIT cells to have  
459 predictive value (Flament et al., 2021). Here we identified a dramatic, early loss of NKT cells  
460 in the circulating immune compartment of COVID-19s. While others confirmed this observation  
461 (Zhang et al., 2020a; Zingaropoli et al., 2020), here we found this phenomenon indeed to not  
462 be shared across severe RS patients but being specific to the SARS-CoV-2 immune response.  
463 NKT cells are important for the production of an early wave of IL-4 promoting germinal center  
464 (GC) formation during viral infection. Delay in GC formation in COVID-19 patients may be a  
465 direct consequence of NKT cell migration to the airways (Dempsey, 2018; Fontana and  
466 Pepper, 2018; Jouan et al., 2020; Kaneko et al., 2020). Translation of this finding into clinical  
467 routine diagnostics can easily be implemented using CD3 and CD56 to calculate NKT cell  
468 frequencies upon hospital admission. Across our three independent COVID-19 cohorts, a cut-  
469 off set to 2.3% for NKT cell frequencies (among T cells) would have identified all patients who  
470 later developed severe disease. Early identification of patients at risk could help to tailor their  
471 treatment and improve the outcome.

## 472 **LIMITATIONS OF THE STUDY**

473 While we initially anticipated center-specific batch effects in our multi-center study, this was  
474 not the case. However, our HAP cohort consists of patients suffering from severe pneumonia

475 driven by multiple pathogens, both bacterial and viral. The comparison of COVID-19 patients  
476 to a pure viral pneumonia cohort could help to further specify the unique immune signatures  
477 to SARS-CoV-2 and distinctive to other viruses. Using PBMCs as source of analyzed immune  
478 cells allows for easy implementation of our findings (such as NKT frequency as predictive  
479 biomarker) to the clinics. Even though the simple measurement of circulating NKT cell  
480 frequencies would have predicted all of our COVID-19 patients who developed severe  
481 disease, larger follow-up studies are needed to solidify this measurement as a predictive  
482 biomarker for COVID-19 patient outcomes.

## 483 **ACKNOWLEDGEMENTS**

484 We thank the patients and blood donors who contributed to this study, and the hospitals at  
485 Nantes, Toulouse and Tübingen for sample and data collection. Regarding specifically the  
486 COVID-BioToul biobank (ClinicalTrials.gov Identifier: NCT04385108) we thank the CRB TBR,  
487 the Clinical Research Center 1436 and the Delegation for clinical research and innovation of  
488 the Toulouse University Hospital for their highly valuable implication. We thank the biological  
489 resource centre for biobanking (CHU Nantes, Nantes Université, Centre de ressources  
490 biologiques (BB-0033-00040), F-44000 Nantes, France).

491 This work was supported by the Swiss National Science Foundation (733 310030\_170320,  
492 310030\_188450 and CRSII5\_183478 to B.B., 31CA30\_195883 to S.Kreutmair, M.C., M.B.  
493 and B.B.), The LOOP Zurich, the Vontobel foundation (to B.B.), the the European Union's  
494 Horizon 2020 research and innovation programme under grant agreement No 847782 (to B.B.  
495 and A.R.) and the European Research Council (ERC; No 882424) to B.B., the Agence National  
496 de la Recherche (ANR) and Region Pays de la Loire – Flash COVID-19:COVARDS project  
497 (to A.R.) and the French Ministry of Health with the participation of the Groupement  
498 Interrégional de Recherche Clinique et d'Innovation Sud-Ouest Outre-Mer (PHRCI 2020  
499 IMMUNOMARK-COV) (to R.L. and G.M.-B.). S.Kreutmair is a recipient of a postdoctoral  
500 fellowship of the Deutsche Forschungsgemeinschaft (DFG). N.G.N. is a recipient of a  
501 University Research Priority Program (URPP) postdoctoral fellowship. F.I. received a PhD  
502 fellowship from the Studienstiftung des deutschen Volkes. We thank Dr. Lucy Robinson from  
503 Insight Editing London for critical review and editing of the manuscript.

## 504 **AUTHOR CONTRIBUTIONS**

505 Conceptualization, B.B., S.Kreutmair, S.U., N.G.N., C.A., D.D.F. and A.R.; Methodology,  
506 S.Kreutmair, S.U., N.G.N. and F.I.; Formal Analysis, S.Kreutmair, S.U., N.G.N., F.I., M.K.,  
507 S.B.; Investigation, S.Kreutmair, S.U., N.G.N., F.I., C.A., D.D.F.; Resources, B.B., A.R., M.B.,  
508 G.M.-B., R.L., M.C.; Sample and patient data collection and processing, S.Kreutmair, B.G.,  
509 I.A., S.A.-H., J.N., M.B., G.M.-B., M.L., N.P.J., M.K., N.P.M., S.G., P.R., H.A.H.; Data Curation,  
510 S.Kreutmair, S.U., N.G.N., F.I., C.A., D.D.F., E.F.; Writing – Original Draft, S.Kreutmair,  
511 S.Krishnarajah and B.B.; Writing – Review & Editing, S.Kreutmair, S.U., N.G.N., F.I., C.A.,  
512 D.D.F., S.Krishnarajah, M.K., E.F., S.B., B.G., M.L., N.P.J., N.P.M., S.G., P.R., H.A.H., I.A.,  
513 S.A.-H., J.N., M.C., R.L., G.M.-B., M.B., A.R. and B.B.; Visualization, S.Kreutmair, N.G.N., F.I.  
514 and M.K.; Funding Acquisition and Supervision, M.C., R.L., G.M.-B., M.B., A.R., and B.B.

515 **FIGURE LEGENDS**

516 **Figure 1: Immunomonitoring reveals differing immune landscapes in COVID-19m,**  
517 **COVID-19s and HAP patients**

518 **A:** Schematic of experimental approach.

519 **B:** UMAP with FlowSOM overlay showing total CD45<sup>pos</sup> cells of combined samples. 1000 cells  
520 were subsetted from every sample from each cohort.

521 **C:** PCA of the total immune compartment based on marker expression in the surface panel.

522 **D:** Comparison of immune features derived from each leukocyte subpopulation between  
523 experimental groups. A dot plot displaying the ES calculated in HAP vs. COVID-19s (x axis;  
524 threshold 0.4) compared to the ES calculated in COVID-19m vs. COVID-19s (y axis; threshold  
525 0.3). Each dot represents one immunological feature, colors represent the leukocyte  
526 compartment they refer to.

527 **E:** Proportion of each immune compartment (normalized to input) in the identified sets of  
528 immune features highlighted in Fig. 1D.

529 See also Figure S1.

530 **Figure 2: Shared T cell features between severe pathogen-induced RSs highlight the**  
531 **emergence of hyperinflammatory and exhausted subsets in COVID-19s**

532 **A:** Comparison of immune features derived from each leukocyte subpopulation between  
533 experimental groups. A dot plot displaying the ES calculated in HAP vs. COVID-19s (x axis;  
534 threshold 0.4) compared to the ES calculated in COVID-19m vs. COVID-19s (y axis; threshold  
535 0.3). Each dot represents one immunological feature. The red box highlights immune features,  
536 which are associated with severe RS (COVID-19s and HAP), with a focus on changes within  
537 the T cell fraction.

538 **B:** UMAP with FlowSOM overlay of total T cells of combined samples. 1000 cells were  
539 subsetted from every sample from each cohort. T cell subsets with transparent names do not  
540 contain immune features highlighted in Fig. 2A.

541 **C:** Median frequencies and 25th and 75th percentile of FlowSOM-generated CD4<sup>+</sup> CD8<sup>-</sup>  
542 (TCR $\gamma\delta$  enriched) immune cell cluster.

543 **D:** Median expression and 25th and 75th percentile of PD-1 in FlowSOM-generated immune  
544 cell clusters shown in B.

545 **E:** Median expression of CTLA-4 within CD4<sup>+</sup> EM T cell subset of HCs shown in grey, of HAP  
546 in blue and of mild and severe COVID-19 patients across TPs 1-5 shown in red.

547 **F:** Schematic overview of cytokine polarization profile comparing COVID-19s and COVID-  
548 19m. UMAP with FlowSOM overlay shows cytokine-producing T cell subpopulations (features  
549 reaching an ES > 0.3). 1000 T cells were subsetted from every sample from each cohort.

550 **G:** Median frequency and 25th and 75th percentile of IFN- $\gamma$  positive cells in FlowSOM-  
551 generated immune cell clusters shown in F.

552 **H:** Median frequency and 25th and 75th percentile of IL-2 positive cells in FlowSOM-generated  
553 immune cell cluster shown in F.

554 **I:** Correlation between frequency of GM-CSF expressing CD4<sup>+</sup> (left panel) and CD8<sup>+</sup> (right  
555 panel) TEMRA cells and the severity grade of COVID-19 patients in combined TPs 1 and 2.

556 **J:** Heatmap depicting the z-score of each T cell related immune feature (highlighted in Fig.  
557 2A) when compared to HCs for every TP. Both negative and positive changes are visualized  
558 by intensity of red color scale. MFI = Mean fluorescence intensity.

559 Significant p values are depicted using an asterisk (\* = p < 0.05, \*\* = p < 0.01, \*\*\* = p < 0.001  
560 and \*\*\*\* = p < 0.0001, Mann-Whitney test, BH correction). See also Figure S2.

561 **Figure 3: Phenotypic alterations in innate immune signatures are shared in severe**  
562 **COVID-19 and HAP**

563 **A:** Comparison of immune features derived from each leukocyte subpopulation between  
564 experimental groups. A dot plot displaying the ES calculated in HAP vs. COVID-19s (x axis;  
565 threshold 0.4) compared to the ES calculated in COVID-19m vs. COVID-19s (y axis; threshold  
566 0.3). Each dot represents one immunological feature. The red box highlights immune features,  
567 which are associated with severe RS, with a focus on changes within the monocyte, DC and  
568 NK cell fraction.

569 **B:** UMAP with FlowSOM overlay of total NK cells of combined samples. 1000 cells were  
570 subsetted from every sample from each cohort. NK cell subsets with transparent names do  
571 not contain immune features highlighted in Fig. 3A.

572 **C:** Median expression of various markers in FlowSOM-derived clusters shown in **B**.

573 **D:** Median expression and 25th and 75th percentile of HLA-DR in FlowSOM-generated  
574 CD56<sup>low</sup> CD16<sup>-</sup> NK cell cluster shown in **B**, combined for TP 1 and 2 (left panel) or displayed  
575 for every individual TP (right panel).

576 **E:** UMAP with FlowSOM overlay of total monocytes and DCs of combined samples. 1000 cells  
577 were subsetted from every sample from each cohort. Monocyte and DC subsets with  
578 transparent names do not contain immune features highlighted in Fig. 3A.

579 **F:** Median expression of various markers in FlowSOM-derived clusters shown in **E**.

580 **G:** Median frequencies and 25th and 75th percentile of FlowSOM-generated pDC immune cell  
581 cluster.

582 **H:** Correlation between median expression of CCR2 in cDC2s following TLR7 and TLR8  
583 stimulation against the severity grade of COVID-19 patients. All TPs have been pooled in the  
584 left panel, and individual TPs depicted in the right panel.

585 **I:** Heatmap depicting the z-score of each monocyte and DC related immune feature  
586 (highlighted in Fig. 3A) when compared to HCs for every TP. Both negative and positive  
587 changes are visualized by intensity of red color scale. MFI = Mean fluorescence intensity.

588 Significant p values are depicted using an asterisk (\* =  $p < 0.05$ , \*\* =  $p < 0.01$ , \*\*\* =  $p < 0.001$   
589 and \*\*\*\* =  $p < 0.0001$ , Mann-Whitney test, BH correction). See also Figure S3.

#### 590 **Figure 4: Impaired antigen-presentation distinguishes the immune response to SARS-** 591 **CoV-2 versus other respiratory pathogens**

592 **A:** Comparison of immune features derived from each leukocyte subpopulation between  
593 experimental groups. A dot plot displaying the ES calculated in HAP vs. COVID-19s (x axis;  
594 threshold 0.4) compared to the ES calculated in COVID-19m vs. COVID-19s (y axis; threshold  
595 0.3). Each dot represents one immunological feature. The red box highlights immune features,  
596 which are different in COVID-19s and HAP, with a focus on changes within monocytes and  
597 DCs.

598 Median expression of HLA-DR (**B**) or CD86 (**C**) within classical monocytes of HCs shown in  
599 grey, HAP patients in blue, and COVID-19m and COVID-19s patients across TPs 1-5 shown  
600 in red.

601 Correlation between median expression of HLA-DR (**D**) or CD86 (**E**) in monocytes or DCs (TP  
602 1 and 2 pooled) against the severity grade of COVID-19 patients.

603 **F:** Heatmap depicting the z-score of each monocyte and DC related immune feature  
604 (highlighted in Fig. 4A) when compared to HCs for every TP. Both negative and positive  
605 changes are visualized by intensity of red color scale.

606 Median expression and the 25th and 75th percentile of HLA-DR (**G**) or CD86 (**H**) in FlowSOM-  
607 generated monocyte and DC immune cell clusters.

608 Significant p values are depicted using an asterisk (\* =  $p < 0.05$ , \*\* =  $p < 0.01$ , \*\*\* =  $p < 0.001$   
609 and \*\*\*\* =  $p < 0.0001$ , Mann-Whitney test, BH correction). See also Figure S4.

610 **Figure 5: Distinct signatures of COVID-19s are exclusive to the lymphocyte**  
611 **compartment**

612 **A:** Comparison of immune features derived from each leukocyte subpopulation between  
613 experimental groups. A dot plot displaying the ES calculated in HAP vs. COVID-19s (x axis;  
614 threshold 0.4) compared to the ES calculated in COVID-19m vs. COVID-19s (y axis; threshold  
615 0.3). Each dot represents one immunological feature. The red box highlights immune features,  
616 which are different in COVID-19s and HAP, with a focus on changes within T and NK cells.

617 **B:** Median frequencies and 25th and 75th percentile of FlowSOM-generated NKT immune cell  
618 cluster.

619 **C:** Correlation between median expression of PD-1 in CD4<sup>+</sup> EM cells (TP 1 and 2 pooled)  
620 against the severity grade of COVID-19 patients.

621 **D:** Correlation between median expression of CD38 in CD4<sup>-</sup> CD8<sup>-</sup> (TCR $\gamma\delta$  enriched) and CD4<sup>+</sup>  
622 EM T cells (TP 1 and 2 pooled) against the severity grade of COVID-19 patients.

623 **E:** Median expression and 25th and 75th percentile of CD161 in FlowSOM-generated CD4<sup>-</sup>  
624 CD8<sup>-</sup> (TCR $\gamma\delta$  enriched) immune cell cluster.

625 **F:** Correlation between median expression of CD95 in CD56<sup>high</sup> NK cells (TP 1 and 2 pooled)  
626 against the severity grade of COVID-19 patients.

627 **G:** Schematic overview of cytokine polarization profile comparing COVID-19s and COVID-  
628 19m. UMAP with FlowSOM overlay shows cytokine-producing T cells (features reaching an  
629 ES > 0.3 vs COVID-19m and > 0.4 vs HAP). 1000 T cells were subsetted from every sample  
630 from each cohort.

631 **H:** Median frequency and 25th and 75th percentile of IFN- $\gamma$  positive cells in FlowSOM-  
632 generated immune cell clusters shown in G.

633 **I:** Heatmap depicting the z-score of each T and NK cell related immune feature (highlighted in  
634 Fig. 5A) when compared to HCs for every TP. Both negative and positive changes are  
635 visualized by intensity of red color scale. MFI = Mean Fluorescence Intensity.

636 **J:** Median frequencies or expression of indicated populations and markers. Boxplots show the  
637 25th and 75th percentile.

638 Significant p values are depicted using an asterisk (\* =  $p < 0.05$ , \*\* =  $p < 0.01$ , \*\*\* =  $p < 0.001$   
639 and \*\*\*\* =  $p < 0.0001$ , Mann-Whitney test, BH correction). See also Figure S5.

640 **Figure 6: HLA profile links COVID-19 immunopathology to impaired virus recognition**

641 **A:** Correlogram of all immune features (TP 1 and 2) with ES COVID-19s vs. COVID-19m >  
642 0.3, shown for COVID-19s and HAP. Red arrows highlight immune features unique in COVID-  
643 19s (ES vs. HAP > 0.4). The black boxes #1-3 highlight highly correlating immune clusters.

644 **B:** Correlogram of immune features from TP 1 only with ES COVID-19s vs. COVID-19m > 0.3  
645 with HLA score 50. HLA score 50 represents the number of predicted tightly binding SARS-  
646 CoV-2 peptides of both HLA alleles of a patient. Red arrows highlight SARS-CoV-2-specific  
647 immune features (ES COVID-19s vs. HAP > 0.4).

648 **C:** Correlogram of immune features from TP 1 only with ES COVID-19s vs. COVID-19m > 0.3  
649 with routinely assessed clinical parameters. Red arrows highlight highly correlating  
650 parameters.

651 **D:** Correlation between LDH and granulocyte counts (TP 1 only) against the severity grade of  
652 COVID-19 patients.

653 See also Figure S6.

654 **Figure 7: ACE2 expression in a CD4+ T cell subset increases after ex vivo stimulation**

655 **A:** Comparison of immune features derived from each leukocyte subpopulation between  
656 experimental groups. A dot plot displaying the ES calculated in HAP vs. COVID-19s (x axis)  
657 compared to the ES calculated in COVID-19m vs. COVID-19s (y axis). Each dot represents  
658 one immunological feature. The red box highlights the immune feature focused in this figure.

659 **B:** Median expression of indicated markers in FlowSOM-derived clusters of unstimulated  
660 samples.

661 **C:** Median frequency and 25th and 75th percentile of ACE2 positive cells in a subset of  
662 unstimulated CXCR3<sup>+</sup> CCR6<sup>+</sup> (Th1 Th17-enriched) CD4<sup>+</sup> T cells. All TPs have been pooled.

663 **D:** Median frequency and 25th and 75th percentile of CXCR3<sup>+</sup> CCR6<sup>+</sup> (Th1 Th17-enriched)  
664 CD4<sup>+</sup> T cells at each TP.

665 **E:** Representative plot showing ACE2 and isotype staining within the T cell compartment of  
666 PMA and ionomycin restimulated (5h) COVID-19 samples.

667 **F:** Median frequency and 25th and 75th percentile of ACE2 positive cells in FlowSOM-  
668 generated immune cell clusters after PMA and ionomycin restimulation (5h). All TPs have  
669 been pooled.

670 **G:** Median expression of various markers in FlowSOM-derived clusters of PMA and ionomycin  
671 restimulated (5h) samples.

672 **H:** Median expression and 25th and 75th percentile of PD-1 (left panel) and CTLA-4 (right  
673 panel) in FlowSOM-generated immune cell clusters after PMA and ionomycin restimulation  
674 (5h). All TPs have been pooled.

675 Significant p values are depicted using an asterisk (\* =  $p < 0.05$ , \*\* =  $p < 0.01$ , \*\*\* =  $p < 0.001$   
676 and \*\*\*\* =  $p < 0.0001$ , Mann-Whitney test, BH correction). See also Figure S7.

## 677 STAR METHODS

## 678 KEY RESOURCES TABLE

REAGENT or RESOURCE	SOURCE	IDENTIFIER
Antibodies		
anti-human ACE2 (Biotin) (AC18F)	Adipogen Life sciences	Cat# AG-20A-0032B-C050; RRID: N/A
anti-human CCR2 (K036C2), BV605	BioLegend	Cat# 357213; RRID:AB_2562702
anti-human CCR6 (G034E3), BV711	BioLegend	Cat# 353435; RRID:AB_2629607
anti-human CCR7 (CD197) (G043H7), BV785	BioLegend	Cat# 353229; RRID:AB_2561371
anti-human CD11c (B-ly6), BUV661	BD	Cat# 612968; RRID:AB_2870241
anti-human CD123 (IL-3R) (6H6), APC/Fire 750	BioLegend	Cat# 306041; RRID:AB_2750163
anti-human CD123 (IL-3R) (6H6), BV711	BioLegend	Cat# 306029; RRID:AB_2566353
anti-human CD14 (M5E2), BUV737	BD	Cat# 612763; RRID:AB_2870094
anti-human CD14 (Tük4), Qdot800	Thermo	Cat# Q10064; RRID:AB_2556449
anti-human CD141 (1A4), BB700	BD	Cat# 742245; RRID:AB_2740668
anti-human CD152 (CTLA-4) (BNI3), BB790-P	BD	customized
anti-human CD16 (3G8), BUV496	BD	Cat# 612944; RRID:AB_2870224
anti-human CD161 (HP-3G10), eFluor 450	Thermo	Cat# 48-1619-41; RRID:AB_10854575
anti-human CD19 (HIB19), APC-Cy7	BioLegend	Cat# 302218; RRID:AB_314248
anti-human CD19 (SJ25C1), PE-Cy5.5	Thermo	Cat# 35-0198-42; RRID:AB_11218903
anti-human CD194 (CCR4) (1G1), BUV615	BD	Cat# 613000; RRID:AB_2870269
anti-human CD1c (F10/21A3), BB660-P2	BD	customized
anti-human CD25 (IL-2Ra) (M-A251), PE-Cy7	BioLegend	Cat# 356107; RRID:AB_2561974
anti-human CD27 (M-T271), BUV563	BD	Cat# 741366; RRID:AB_2870866
anti-human CD279 (PD-1) (EH12.2H7), BV421	BioLegend	Cat# 329919; RRID:AB_10900818
anti-human CD279 (PD-1) (EH12.2H7), BV605	BioLegend	Cat# 329924; RRID:AB_2563212
anti-human CD28 (CD28.2), BV605	BioLegend	Cat# 302967; RRID:AB_2800754
anti-human CD3 (HIT3a), APC-Cy7	BioLegend	Cat# 300318; RRID:AB_314054
anti-human CD3 (Oct.03), BV510	BioLegend	Cat# 317332; RRID:AB_2561943
anti-human CD3 (UCHT1), BUV805	BD	Cat# 565515; RRID:AB_2739277
anti-human CD33 (WM53), BUV395	BD	Cat# 740293; RRID:AB_2740032
anti-human CD38 (HIT2), APC-Cy5.5	Thermo	Cat# MHCD3819; RRID:AB_1472718

anti-human CD4 (SK3), Spark Blue 550	BioLegend	Cat# 344656; RRID:AB_2819979
anti-human CD45 (2D1), PerCP	BioLegend	Cat# 368506; RRID:AB_2566358
anti-human CD45 (HI-30), BUV805	BD	Cat# 564915; RRID:AB_2744401
anti-human CD45RA (HI100), BUV395	BD	Cat# 740298; RRID:AB_2740037
anti-human CD56 (HCD56), APC-Cy7	BioLegend	Cat# 318332; RRID:AB_10896424
anti-human CD56 (NCAM16.2), BUV737	BD	Cat# 612766; RRID:AB_2813880
anti-human CD57 (HNK-1), FITC	BioLegend	Cat# 359603; RRID:AB_2562386
anti-human CD8 (3B5), Ax Fluor 700	Thermo	Cat# MHCD0829; RRID:AB_10372957
anti-human CD86 (2331 (FUN-1)), BUV805	BD	Cat# 742032; RRID:AB_2871328
anti-human CD95 (FasR) (DX2), PE/Cy5	Thermo	Cat# 15-0959-42; RRID:AB_11042290
anti-human CXCR3 (G025H7), BV650	BioLegend	Cat# 353729; RRID:AB_2562628
anti-human CXCR5 (CD185) (RF8B2), BV750	BD	Cat# 747111; RRID:AB_2871862
anti-human GM-CSF (BVD2-21C11), PE	BD	Cat# 554507; RRID:AB_395440
anti-human Granzyme B (GB11), FITC	BioLegend	Cat# 515403; RRID:AB_2114575
anti-human HLA-DR (L243), BV570	BioLegend	Cat# 307637; RRID:AB_10895753
anti-human IFN- $\gamma$ (B27),V450	BD	Cat# 560371; RRID:AB_1645594
anti-human IgD (IA6-2), BV480	BD	Cat# 566138; RRID:AB_2739536
anti-human IgG (polyclonal), Ax Fluor 647	Jackson immuno research	Cat# 109-606-098; RRID:AB_2337899
anti-human IgM (MHM-88), PE/Dazzle594	BioLegend	Cat# 314529; RRID:AB_2566482
anti-human IL-17A (BL168), APC-Cy7	BioLegend	Cat# 512320; RRID:AB_10613103
anti-human IL-1 $\beta$ (H1b-98), Pacific Blue	BioLegend	Cat# 511710; RRID:AB_2124350
anti-human IL-2 (MQ1-17H12), BV711	BioLegend	Cat# 500345; RRID:AB_2616638
anti-human IL-21 (3A3-N2.1), Ax Fluor 647	BD	Cat# 562043; RRID:AB_10896655
anti-human IL-4 (8D4-8), APC	BioLegend	Cat# 500714; RRID:AB_1877159
anti-human IL-6 (MQ2-13A5), PE/Dazzle594	BioLegend	Cat# 501122; RRID:AB_2810622
anti-human IL-8 (E8N1), PE-Cy7	BioLegend	Cat# 511415; RRID:AB_2565290
anti-human TCR $\gamma\delta$ (IMMU510), Pe-Cy5	Beckman Coulter	Cat# IM2662U; RRID: N/A
anti-human TNF (MAb11), BV750	BD	Cat# 566359; RRID:AB_2739709
Streptavidin, BB630-P2	BD	customized
Biological samples		

COVID-19 PBMC samples	University Hospital Tuebingen, Germany	N/A
COVID-19 PBMC samples	Toulouse University Hospital, France	N/A
COVID-19 PBMC samples	Nantes University Hospital, France	N/A
HAP PBMC samples	Nantes University Hospital, France	N/A
Healthy PBMC samples	Nantes University Hospital, France	N/A
Chemicals, peptides, and recombinant proteins		
RPMI 1640	Seraglob	Cat# M3413; RRID: N/A
Phosphate-buffered saline	Homemade	N/A
R848	Invivogen	Cat# tlr-r848; RRID: N/A
Human TruStain FcX	BioLegend	Cat# 422302; RRID:AB_2818986
Formaldehyde 4.0%	PanReac	Cat# 252931.1211; RRID: N/A
Benzonase nuclease	Sigma-Aldrich	Cat# E1014-25KU; RRID: N/A
Fetal bovine serum	Gibco	Cat# A3160802; RRID: N/A
Penicillin Streptomycin	Gibco	Cat# 15140-148; RRID: N/A
GlutaMAX	Gibco	Cat# 35050-038; RRID: N/A
Phorbol 12-myristate 13-acetate	Sigma-Aldrich	Cat# P1585-1MG; RRID: N/A
Ionomycin	Sigma-Aldrich	Cat# I0634-1MG; RRID: N/A
1x Brefeldin A	BD	Cat# 555029; RRID:AB_2869014
1x Monensin	BD	Cat# 554724; RRID:AB_2869012
Live/Dead Fixable Blue	Thermo Scientific	Cat# L23105; RRID: N/A
DNA easy blood and tissue kit	Quiagen	Cat# 69504; RRID: N/A
Deposited data		
spectral flow cytometry data	this study	<a href="http://dx.doi.org/10.17632/ffkvft27ds.2">http://dx.doi.org/10.17632/ffkvft27ds.2</a>
supplemental spreadsheets	this study	<a href="http://dx.doi.org/10.17632/ffkvft27ds.2">http://dx.doi.org/10.17632/ffkvft27ds.2</a>
scRNA-seq data	(Zhao et al., 2021)	<a href="https://www.ncbi.nlm.nih.gov/geo/query/acc.cgi?acc=GSE167118">https://www.ncbi.nlm.nih.gov/geo/query/acc.cgi?acc=GSE167118</a>
Software and algorithms		
Affinity designer	Affinity	<a href="https://affinity.serif.com/de/designer/">https://affinity.serif.com/de/designer/</a>
corrplot	Taiyun Wei and Viliam Simko (2017)	<a href="https://github.com/taiyun/corrplot">https://github.com/taiyun/corrplot</a>
dplyr	Wickham et al., 2019	<a href="https://cran.r-project.org/web/packages/dplyr/index.html">https://cran.r-project.org/web/packages/dplyr/index.html</a>

FlowJo V10.6.2.	Tree Star	<a href="https://www.flowjo.com/">https://www.flowjo.com/</a>
FlowSOM	(Van Gassen et al., 2015)	<a href="https://github.com/SoefieVG/FlowSOM">https://github.com/SoefieVG/FlowSOM</a>
flowStats	Hahne et al., 2020	<a href="https://www.bioconductor.org/packages/release/bioc/html/flowStats.html">https://www.bioconductor.org/packages/release/bioc/html/flowStats.html</a>
ggplot2	Wickham et al., 2019	<a href="https://cran.r-project.org/web/packages/ggplot2/index.html">https://cran.r-project.org/web/packages/ggplot2/index.html</a>
Harmony	(Korsunsky et al., 2019)	<a href="https://github.com/immunogenomics/harmony">https://github.com/immunogenomics/harmony</a>
Hmisc	Harrell, 2020	<a href="https://cran.r-project.org/web/packages/Hmisc/index.html">https://cran.r-project.org/web/packages/Hmisc/index.html</a>
pheatmap	Kolde, 2019	<a href="https://cran.r-project.org/web/packages/pheatmap/index.html">https://cran.r-project.org/web/packages/pheatmap/index.html</a>
R studio	(R Studio, 2015)	<a href="https://www.rstudio.com/">https://www.rstudio.com/</a>
R version 3.6.1	(R Core, 2013)	<a href="https://www.r-project.org/">https://www.r-project.org/</a>
Seurat (v3.1.4)	(Stuart et al., 2019)	<a href="https://satijalab.org/seurat/">https://satijalab.org/seurat/</a>
SingleR	(Aran et al., 2019)	<a href="https://github.com/dviraran/SingleR">https://github.com/dviraran/SingleR</a>
Stats	Bolar et al., 2019	<a href="https://CRAN.R-project.org/package=STAT">https://CRAN.R-project.org/package=STAT</a>
UMAP	(McInnes et al., 2018)	<a href="https://github.com/mcinnnes/umap">https://github.com/mcinnnes/umap</a>
Other		
Automated cell counter	Bio-Rad	N/A
Cryo thaw devices	Medax	N/A
Cytek Aurora	Cytek Biosciences	N/A
Illumina MiniSeq	Illumina	N/A
LABScan 3D instrument	Luminex	N/A

679

680 **RESOURCE AVAILABILITY**

681 **Lead Contact**

682 Further information and requests for resources should be directed to and will be fulfilled by the  
683 Lead Contact, Burkhard Becher (becher@immunology.uzh.ch).

684 **Materials Availability**

685 This study did not generate new unique reagents.

## 686 **Data and Code Availability**

687 Spectral flow cytometry data generated during this study and additional supplemental items  
688 are available from Mendeley Data at <http://dx.doi.org/10.17632/ffkvft27ds.2> (DOI:  
689 10.17632/ffkvft27ds.2)

## 690 **EXPERIMENTAL MODEL AND SUBJECT DETAILS**

### 691 **COVID-19 Patient Samples**

692 Clinical routine data and blood samples for peripheral blood mononuclear cell (PBMC)  
693 isolation and cryopreservation were collected at the University Hospital Tuebingen (Germany),  
694 the Toulouse University Hospital (France, in the frame of the COVID-BioToul biobank,  
695 ClinicalTrials.gov Identifier: NCT04385108) and the Nantes University Hospital (France)  
696 (Table S1A). All donors had given written informed consent and the study was approved by  
697 the regional ethical review board of Tuebingen (COVID-19), Toulouse (COVID-19) and Nantes  
698 (COVID-19, HAP, Healthy) respectively. COVID-19 diagnosis was established by a positive  
699 PCR test. PBMC samples were collected longitudinally at the indicated time points post-  
700 admission to the hospital (Table S1C). COVID-19 patients were graded according to the  
701 maximum severity of disease during the study based on the WHO ordinal scale (World Health  
702 Organization, 2020b). The WHO grade 1 and 2 were combined to grade 1 in our scale, the  
703 WHO grade 7 and 8 were combined to grade 6 in our categorization. The appropriate severity  
704 grade was then allocated to all samples of the same patient. Mean age of COVID-19 patients  
705 was 62.2 years, the percentage of females was 40.4.

### 706 **Human Subjects with HAP and Healthy Samples**

707 Bioresources: IBIS-sepsis (severe septic patients) and IBIS (brain-injured patients), Nantes,  
708 France. Patients were enrolled from January 2016 to May 2019 in two French Surgical  
709 Intensive Care Units of one University Hospital (Nantes, France) and samples collected in  
710 accordance to the guideline of standardization (CoBRA) (Bravo et al., 2015). Patients with  
711 immunosuppression were not enrolled to the study. The criteria to diagnose hospital-acquired  
712 pneumonia were (1) radiological signs combined with (2) body temperature  $> 38,3^{\circ}\text{C}$  without  
713 any other cause or leukocytes  $< 4000/\text{mm}^3$  or  $> 12000/\text{mm}^3$  and (3) at least two of the following  
714 symptoms: purulent sputum, cough or dyspnea, declining oxygenation or increased oxygen-  
715 requirement or need for respiratory assistance (Leone et al., 2018). Hospital-acquired  
716 pneumonia were microbiologically confirmed with quantitative culture (for patients with  
717 antibiotics  $< 48\text{h}$ ) (thresholds of  $10^4$  colony-forming units (CFU) per mL for a bronchoalveolar  
718 lavage). PCR for Herpes Simplex Virus and Cytomegalovirus were performed in tracheal  
719 aspirates at day 1, day 7 and day 15 after ICU admission. The collection of human samples  
720 has been declared to the French Ministry of Health (DC-2011-1399), and it has been approved

721 by an institutional review board. Written informed consent from a next-of-kin was required for  
722 enrolment. Retrospective consent was obtained from patients, when possible. All patients  
723 were clinically followed up for 28 days. Control samples were collected from healthy blood  
724 donors, recruited at the Blood Transfusion Center (Etablissement Français du Sang, Nantes,  
725 France). Mean age of HAP patients was 43.8 years, the percentage of females was 8.7. Mean  
726 age of healthy controls was 52.0 years, the percentage of both females was 44.4.

## 727 **METHOD DETAILS**

### 728 ***Ex vivo* Reactivation of PBMCs**

729 PBMCs collected in clinics were kept in cell culture medium (RPMI-1640, 10% fetal bovine  
730 serum (FBS; Gibco), and 1× l-glutamine (Gibco) and 1× penicillin streptomycin (Gibco))  
731 supplemented with 5U ml<sup>-1</sup> benzonase (Sigma–Aldrich) and frozen in liquid nitrogen until  
732 experimental analysis. Then, for spectral flow analysis, cells were thawed using Cryo thaw  
733 devices (Medax). Briefly, cells were resuspended in cell culture medium supplemented with  
734 2U ml<sup>-1</sup> benzonase by centrifugation (300 r.c.f.; 7 min; 24 °C). Cell count was calculated using  
735 an automated cell counter (Bio-Rad). Due to the resulting cell count, cells were used for all  
736 panels or surface panel only. Subsequent procedure including short-term reactivation of  
737 cryopreserved PBMCs and cytometry analysis were performed as described previously (Galli  
738 et al., 2019; Hartmann et al., 2016). Briefly, 2 million (mio) cells were directly stained for  
739 cytometry analysis (surface panel), while 1 mio cells were restimulated with 50 ng ml<sup>-1</sup> phorbol  
740 12-myristate 13-acetate (Sigma–Aldrich) and 500 ng ml<sup>-1</sup> ionomycin (Sigma–Aldrich) in the  
741 presence of 1× Brefeldin A and 1x Monensin (both BD Biosciences) for 5 h at 37°C or in case  
742 of R848 stimulation, 2.5 mio cells using 2µg ml<sup>-1</sup> R848 (Invivogen) in the presence of 1×  
743 Brefeldin A and 1x Monensin (both BD Biosciences) for 8 h at 37°C.

### 744 **Surface Labeling for Spectral Flow Cytometry**

745 For spectral cytometry, samples were washed in PBS and then resuspended in 100µl of Live  
746 Dead Fixable Blue mixture (Thermo Scientific, 1:500) followed by a washing step. To avoid  
747 nonspecific binding, the samples were resuspended in 30 µl of True Stain FcX (BioLegend)  
748 and incubated for 10 min at 4°C. Anti-human flow cytometric antibodies were purchased pre-  
749 conjugated (Table S2A-C). 70 µl of the first surface-antibody mixture was added and cells  
750 were incubated for 15 min at 37°C (Table S2A). After another washing step, the second  
751 surface-antibody staining step (100 µl) was performed for 15 min at 4°C (Table S2A). Then,  
752 fixation was performed using 150 µl of 2% PFA for 15 min at 4°C.

### 753 **Intracellular Cytokine Labeling for Spectral Flow Cytometry**

754 For intracellular spectral cytometry, after surface-antibody labeling, cells were fixed and  
755 permeabilized using Cytofix Cytoperm reagent (BD Biosciences) for 30 min at 4°C.  
756 Intracellular labeling was then performed in 100 µl of 1x permeabilization buffer (Thermo  
757 Scientific) for 11 h (Lymphoid cytokine panel, Table S2B) or 10 h (Myeloid cytokine panel,  
758 Table S2C) at 4°C.

## 759 **HLA Typing**

760 For DNA extraction the DNA easy blood and tissue kit from Quiagen was used. HLA typing  
761 was performed using next generation sequencing (NGS) with the NGSgo-AmpX v2 HLA kits  
762 (GenDx, Utrecht, Netherlands), and sequenced on an Illumina MiniSeq (Illumina, San Diego,  
763 CA). Sequence data were analyzed with NGSengine (GenDx, Utrecht, Netherlands). For  
764 samples with low DNA amount, HLA typing was also performed using sequence specific  
765 oligomers (SSO) with the LABType kits (One Lambda, Canoga Park, CA). The bead-based  
766 analysis was run on a LABScan 3D instrument (Luminex, Austin, TX) and analyzed using the  
767 Fusion Software (One Lambda, Canoga Park, CA). All assays were performed according to  
768 the manufacturer's recommendations.

## 769 **QUANTIFICATION AND STATISTICAL ANALYSIS**

### 770 **Acquisition and Preprocessing of Spectral Flow Cytometry Data**

771 Spectral cytometry samples were acquired on a Cytex Aurora (Cytex Biosciences). Quality  
772 control of the Cytex Aurora was performed daily as instructed by the manufacturer. For  
773 downstream analysis, dead cells and doublets were excluded using FlowJo (TreeStar).  
774 Samples with viability lower than 10% and fewer than 500 live, CD45 positive cells were  
775 excluded. Cytometry data were transformed with an inverse hyperbolic sine (arcsinh) function  
776 using the R environment (range 30 - 18000). To balance the influence of markers with different  
777 dynamic ranges, we performed background subtraction and channel-based percentile  
778 normalization using the 99.9th percentile of each marker across the whole dataset (Bendall et  
779 al., 2011). Individual cytokine positivity thresholds were determined based on the 99<sup>th</sup>  
780 percentile of the residual staining in an unstimulated or isotype-stained control sample.

### 781 **Algorithm-based High-dimensional Analysis of Spectral Flow Cytometry Data**

782 Pre-processed data were downsampled to a maximum of 150'000 cells per donor for the  
783 analysis of the main populations, all cells were used for analysis of the specific immune  
784 compartments. The high dimensional analysis was carried out using the R environment, based  
785 loosely on the workflow described previously (Mair et al., 2016). Two-dimensional UMAP  
786 (Uniform Manifold Approximation and Projection) projections were calculated using the *umap*  
787 package (McInnes L Saul N, Großberger L, 2018). All FlowSOM-based clustering was

788 performed on the whole dataset to enable identification of small populations, and the results  
789 were overlaid on the dimensionality reduction maps (Van Gassen et al., 2015). Principal  
790 component analysis was carried out in the *stats* package using the median activation marker  
791 expression of all detected leukocyte subsets. The circles represent the core areas added by  
792 the default confidence interval of 68%, which facilitates the separation based on the PC1/2  
793 explanatory rate of the overall difference in measured immune features. For the correlogram,  
794 Pearson's r correlation coefficients were computed using the *Hmisc* package and the resulting  
795 correlation matrix was visualized using the *corrplot* package. All other plots were drawn using  
796 *ggplot2*. For longitudinal visualization, smoothed conditional mean of the feature from the  
797 combined COVID-19 cohort was added in light grey.

### 798 **Calculation of HLA Score 50**

799 Based on the study data of Nguyen et al. (Nguyen et al., 2020), the predicted HLA class I  
800 binding capacity to SARS-CoV-2-derived peptides per patient was calculated by counting the  
801 number of all SARS-CoV-2-derived peptides which were predicted to be bound by each  
802 specific HLA allele. The score 50 includes all SARS-CoV-2 peptides which were predicted for  
803 tight binding (<50nm) to the indicated HLA class I allele. The final HLA score 50 per patient  
804 represents the total number of tight binding SARS-CoV-2 peptides of both alleles of the patient  
805 for HLA-A, HLA-B or HLA-C.

### 806 **Single-cell RNA-seq Analysis**

807 For single-cell RNA-seq analysis we used a publicly available dataset of sorted CD45<sup>+</sup> blood  
808 cells of COVID-19 patients  
809 (<https://www.ncbi.nlm.nih.gov/geo/query/acc.cgi?acc=GSE167118>), of which 5'-RNA single  
810 cell transcriptome (10x genomics) was performed. For preprocessing, the feature-barcode  
811 matrices for all the sample were further processed by the R package Seurat (v3.1.4). As a  
812 quality-control (QC) step, we first filtered out the cells in which less than 200 genes were  
813 detected in the blood samples. To remove potential doublets, we excluded cells with total  
814 number of detected genes more than 5000. Low-quality cells with more than 5% mitochondrial  
815 genes of all detected genes were removed. The LogNormalize method in Seurat was used to  
816 normalize the scRNA-seq and batch effect correction was performed using Harmony. The R  
817 package SingleR, an automatic annotation method for single-cell RNA sequencing (Aran et  
818 al., 2019) were then used to determine the cell types. The differential expression between  
819 selected groups were calculated by the FindAllMarkers function (min.pct = 0.25,  
820 logfc.threshold = 0.25, Wilcoxon rank sum tests).

### 821 **Statistical Analysis**

822 Frequencies of immune populations, cytokines, median expression values and absolute  
823 counts were compared with the non-parametric Mann–Whitney–Wilcoxon test and Benjamini-  
824 Hochberg correction for multiple testing, using the R package *rstatix*. For correlation  
825 measurements, we used a linear regression model by applying the *lm()* and *summary()*  
826 functions. P values of less than 0.05 were considered significant and are indicated by an  
827 asterisk (\*) or the numerical value on the respective graphs.

828 **SUPPLEMENTAL TABLES**

829 Detailed information about patient cohorts, clinical routine parameter and TPs (related to  
830 Figure 1A and S1A): Kreutmair\_et\_al\_Suppl\_Table1.xlsx

831 Spectral flow cytometry panels (related to Figure 1-7 and S1-S7):  
832 Kreutmair\_et\_al\_Suppl\_Table2.xlsx

833 Selected immune features (related to Figure 2-5): Kreutmair\_et\_al\_Suppl\_Table3.xlsx

834 ROC curve of NKT cell frequency among T cells (related to Figure 5B):  
835 Kreutmair\_et\_al\_Suppl\_Table4.xlsx

836 HLA types and HLA scores 50 (related to Figure 6B, S6A and S6B):  
837 Kreutmair\_et\_al\_Suppl\_Table5.xlsx

838 **DECLARATION OF INTERESTS**

839 The authors declare no competing interests.

840 **REFERENCES**

- 841 Ackermann, M., Verleden, S.E., Kuehnel, M., Haverich, A., Welte, T., Laenger, F.,  
842 Vanstapel, A., Werlein, C., Stark, H., Tzankov, A., et al. (2020). Pulmonary Vascular  
843 Endothelialitis, Thrombosis, and Angiogenesis in Covid-19. *N. Engl. J. Med.* 383, 120–128.
- 844 Ahmadzadeh, M., Johnson, L.A., Heemskerk, B., Wunderlich, J.R., Dudley, M.E., White,  
845 D.E., and Rosenberg, S.A. (2009). Tumor antigen-specific CD8 T cells infiltrating the tumor  
846 express high levels of PD-1 and are functionally impaired. *Blood* 114, 1537–1544.
- 847 Aran, D., Looney, A.P., Liu, L., Wu, E., Fong, V., Hsu, A., Chak, S., Naikawadi, R.P.,  
848 Wolters, P.J., Abate, A.R., et al. (2019). Reference-based analysis of lung single-cell  
849 sequencing reveals a transitional profibrotic macrophage. *Nat. Immunol.* 20, 163–172.
- 850 Armstrong, R.A., Kane, A.D., and Cook, T.M. (2020). Outcomes from intensive care in  
851 patients with COVID-19: a systematic review and meta-analysis of observational studies.  
852 *Anaesthesia* 75, 1340–1349.
- 853 Arunachalam, P.S., Wimmers, F., Mok, C.K.P., Perera, R.A.P.M., Scott, M., Hagan, T.,  
854 Sigal, N., Feng, Y., Bristow, L., Tak-Yin Tsang, O., et al. (2020). Systems biological  
855 assessment of immunity to mild versus severe COVID-19 infection in humans. *Science* 369,  
856 1210–1220.
- 857 Bastard, P., Rosen, L.B., Zhang, Q., Michailidis, E., Hoffmann, H.-H., Zhang, Y., Dorgham,  
858 K., Philippot, Q., Rosain, J., Béziat, V., et al. (2020). Autoantibodies against type I IFNs in  
859 patients with life-threatening COVID-19. *Science* (80-. ). 370, eabd4585.
- 860 Bendall, S.C., Simonds, E.F., Qiu, P., Amir el, A.D., Krutzik, P.O., Finck, R., Bruggner, R. V,  
861 Melamed, R., Trejo, A., Ornatsky, O.I., et al. (2011). Single-cell mass cytometry of  
862 differential immune and drug responses across a human hematopoietic continuum. *Science*  
863 (80-. ). 332, 687–696.
- 864 De Biasi, S., Meschiari, M., Gibellini, L., Bellinazzi, C., Borella, R., Fidanza, L., Gozzi, L.,  
865 Iannone, A., Lo Tartaro, D., Mattioli, M., et al. (2020). Marked T cell activation, senescence,  
866 exhaustion and skewing towards TH17 in patients with COVID-19 pneumonia. *Nat.*  
867 *Commun.* 11, 3434.
- 868 Bonaventura, A., Vecchié, A., Wang, T.S., Lee, E., Cremer, P.C., Carey, B., Rajendram, P.,  
869 Hudock, K.M., Korbee, L., Van Tassell, B.W., et al. (2020). Targeting GM-CSF in COVID-19  
870 Pneumonia: Rationale and Strategies. *Front. Immunol.* 11, 1625.
- 871 Bosteels, C., Maes, B., Van Damme, K., De Leeuw, E., Declercq, J., Delporte, A.,  
872 Demeyere, B., Vermeersch, S., Vuylsteke, M., Willaert, J., et al. (2020). Sargramostim to  
873 treat patients with acute hypoxic respiratory failure due to COVID-19 (SARPAC): A

874 structured summary of a study protocol for a randomised controlled trial. *Trials* 21, 491.

875 Bravo, E., Calzolari, A., De Castro, P., Mabile, L., Napolitani, F., Rossi, A.M., and Cambon-  
876 Thomsen, A. (2015). Developing a guideline to standardize the citation of bioresources in  
877 journal articles (CoBRA). *BMC Med.* 13, 33.

878 Cao, X. (2020). COVID-19: immunopathology and its implications for therapy. *Nat. Rev.*  
879 *Immunol.* 20, 269–270.

880 chen, yongwen, Feng, Z., Diao, B., Wang, R., Wang, G., Wang, C., Tan, Y., Liu, L., Wang,  
881 C., Liu, Y., et al. (2020). The Novel Severe Acute Respiratory Syndrome Coronavirus 2  
882 (SARS-CoV-2) Directly Decimates Human Spleens and Lymph Nodes. *MedRxiv*  
883 2020.03.27.20045427.

884 Chen, Z., and Wherry, E.J. (2020). T cell responses in patients with COVID-19. *Nat. Rev.*  
885 *Immunol.* 20, 529–536.

886 Cohen, J. (1977). Preface to the Original Edition. In *Statistical Power Analysis for the*  
887 *Behavioral Sciences*, J.B.T.-S.P.A. for the B.S. Cohen, ed. (Academic Press), pp. xiii–xv.

888 Crawford, A., Angelosanto, J.M., Kao, C., Doering, T.A., Odorizzi, P.M., Barnett, B.E., and  
889 Wherry, E.J. (2014). Molecular and transcriptional basis of CD4<sup>+</sup> T cell dysfunction during  
890 chronic infection. *Immunity* 40, 289–302.

891 Dempsey, L.A. (2018). NKT cells aid antiviral responses. *Nat. Immunol.* 19, 99.

892 Ellinghaus, D., Degenhardt, F., Bujanda, L., Buti, M., Albillos, A., Invernizzi, P., Fernández,  
893 J., Prati, D., Baselli, G., Asselta, R., et al. (2020). Genomewide Association Study of Severe  
894 Covid-19 with Respiratory Failure. *N. Engl. J. Med.*

895 Erokhina, S.A., Streltsova, M.A., Kanevskiy, L.M., Grechikhina, M. V, Sapozhnikov, A.M.,  
896 and Kovalenko, E.I. (2020). HLA-DR-expressing NK cells: Effective killers suspected for  
897 antigen presentation. *J. Leukoc. Biol.*

898 Fergusson, J.R., Smith, K.E., Fleming, V.M., Rajoriya, N., Newell, E.W., Simmons, R.,  
899 Marchi, E., Björkander, S., Kang, Y.-H., Swadling, L., et al. (2014). CD161 defines a  
900 transcriptional and functional phenotype across distinct human T cell lineages. *Cell Rep.* 9,  
901 1075–1088.

902 Fergusson, J.R., Hühn, M.H., Swadling, L., Walker, L.J., Kurioka, A., Llibre, A., Bertoletti, A.,  
903 Holländer, G., Newell, E.W., Davis, M.M., et al. (2016). CD161(int)CD8<sup>+</sup> T cells: a novel  
904 population of highly functional, memory CD8<sup>+</sup> T cells enriched within the gut. *Mucosal*  
905 *Immunol.* 9, 401–413.

906 Flament, H., Rouland, M., Beaudoin, L., Toubal, A., Bertrand, L., Lebourgeois, S.,

907 Rousseau, C., Soulard, P., Gouda, Z., Cagninacci, L., et al. (2021). Outcome of SARS-CoV-  
908 2 infection is linked to MAIT cell activation and cytotoxicity. *Nat. Immunol.* 22, 322–335.

909 Fontana, M.F., and Pepper, M. (2018). NKTeeing Up B Cell Responses to Viral Infection.  
910 *Immunity* 48, 198–200.

911 Galli, E., Friebel, E., Ingelfinger, F., Unger, S., Núñez, N.G., and Becher, B. (2019). The end  
912 of omics? High dimensional single cell analysis in precision medicine. *Eur. J. Immunol.* 49,  
913 212–220.

914 Van Gassen, S., Callebaut, B., Van Helden, M.J., Lambrecht, B.N., Demeester, P., Dhaene,  
915 T., and Saeys, Y. (2015). FlowSOM: Using self-organizing maps for visualization and  
916 interpretation of cytometry data. *Cytom. Part A* 87, 636–645.

917 Hadjadj, J., Yatim, N., Barnabei, L., Corneau, A., Boussier, J., Pere, H., Charbit, B., Bondet,  
918 V., Chenevier-Gobeaux, C., Breillat, P., et al. (2020). Impaired type I interferon activity and  
919 exacerbated inflammatory responses in severe Covid-19 patients. *MedRxiv*  
920 2020.04.19.20068015.

921 Han, M., Xu, M., Zhang, Y., Liu, Z., Li, S., He, T., Li, J., Gao, Y., Liu, W., Li, T., et al. (2020).  
922 Assessing SARS-CoV-2 RNA levels and lymphocyte/T cell counts in COVID-19 patients  
923 revealed initial immune status as a major determinant of disease severity. *Med. Microbiol.*  
924 *Immunol.* 209, 657–668.

925 Hartmann, F.J., Bernard-Valnet, R., Queriaux, C., Mrdjen, D., Weber, L.M., Galli, E., Krieg,  
926 C., Robinson, M.D., Nguyen, X.H., Dauvilliers, Y., et al. (2016). High-dimensional single-cell  
927 analysis reveals the immune signature of narcolepsy. *J Exp Med* 213, 2621–2633.

928 Huang, A.C., Orlowski, R.J., Xu, X., Mick, R., George, S.M., Yan, P.K., Manne, S., Kraya,  
929 A.A., Wubbenhorst, B., Dorfman, L., et al. (2019a). A single dose of neoadjuvant PD-1  
930 blockade predicts clinical outcomes in resectable melanoma. *Nat. Med.* 25, 454–461.

931 Huang, H., Wang, S., Jiang, T., Fan, R., Zhang, Z., Mu, J., Li, K., Wang, Y., Jin, L., Lin, F., et  
932 al. (2019b). High levels of circulating GM-CSF(+)CD4(+) T cells are predictive of poor  
933 outcomes in sepsis patients: a prospective cohort study. *Cell. Mol. Immunol.* 16, 602–610.

934 Iadecola, C., Anrather, J., and Kamel, H. (2020). Effects of COVID-19 on the Nervous  
935 System. *Cell* 183, 16-27.e1.

936 Iturrieta-Zuazo, I., Rita, C.G., García-Soidán, A., de Malet Pintos-Fonseca, A., Alonso-  
937 Alarcón, N., Pariente-Rodríguez, R., Tejeda-Velarde, A., Serrano-Villar, S., Castañer-  
938 Alabau, J.L., and Nieto-Gañán, I. (2020). Possible role of HLA class-I genotype in SARS-  
939 CoV-2 infection and progression: A pilot study in a cohort of Covid-19 Spanish patients.

940 Clin. Immunol. 219, 108572.

941 lype, E., and Gulati, S. (2020). Understanding the asymmetric spread and case fatality rate  
942 (CFR) for COVID-19 among countries. MedRxiv 2020.04.21.20073791.

943 Jouan, Y., Guillon, A., Gonzalez, L., Perez, Y., Boisseau, C., Ehrmann, S., Ferreira, M.,  
944 Daix, T., Jeannet, R., François, B., et al. (2020). Phenotypical and functional alteration of  
945 unconventional T cells in severe COVID-19 patients. J. Exp. Med. 217.

946 Kaneko, N., Kuo, H.-H., Boucau, J., Farmer, J.R., Allard-Chamard, H., Mahajan, V.S.,  
947 Piechocka-Trocha, A., Lefteri, K., Osborn, M., Bals, J., et al. (2020). Loss of Bcl-6-  
948 Expressing T Follicular Helper Cells and Germinal Centers in COVID-19. Cell 183, 143-  
949 157.e13.

950 Korsunsky, I., Millard, N., Fan, J., Slowikowski, K., Zhang, F., Wei, K., Baglaenko, Y.,  
951 Brenner, M., Loh, P.-R., and Raychaudhuri, S. (2019). Fast, sensitive and accurate  
952 integration of single-cell data with Harmony. Nat. Methods 16, 1289–1296.

953 Kuri-Cervantes, L., Pampena, M.B., Meng, W., Rosenfeld, A.M., Ittner, C.A.G., Weisman,  
954 A.R., Agyekum, R., Mathew, D., Baxter, A.E., Vella, L., et al. (2020). Immunologic  
955 perturbations in severe COVID-19/SARS-CoV-2 infection. BioRxiv Prepr. Serv. Biol.

956 Kvedaraite, E., Hertwig, L., Sinha, I., Ponzetta, A., Hed Myrberg, I., Lourda, M., Dzidic, M.,  
957 Akber, M., Klingstrom, J., Folkesson, E., et al. (2020). Perturbations in the mononuclear  
958 phagocyte landscape associated with COVID-19 disease severity. MedRxiv  
959 2020.08.25.20181404.

960 Lang, F.M., Lee, K.M.-C., Teijaro, J.R., Becher, B., and Hamilton, J.A. (2020). GM-CSF-  
961 based treatments in COVID-19: reconciling opposing therapeutic approaches. Nat. Rev.  
962 Immunol. 20, 507–514.

963 Lauer, S.A., Grantz, K.H., Bi, Q., Jones, F.K., Zheng, Q., Meredith, H.R., Azman, A.S.,  
964 Reich, N.G., and Lessler, J. (2020). The Incubation Period of Coronavirus Disease 2019  
965 (COVID-19) From Publicly Reported Confirmed Cases: Estimation and Application. Ann.  
966 Intern. Med. 172, 577–582.

967 Lee, J.S., Park, S., Jeong, H.W., Ahn, J.Y., Choi, S.J., Lee, H., Choi, B., Nam, S.K., Sa, M.,  
968 Kwon, J.-S., et al. (2020). Immunophenotyping of COVID-19 and influenza highlights the role  
969 of type I interferons in development of severe COVID-19. Sci. Immunol. 5.

970 Leone, M., Bouadma, L., Bouhemad, B., Brissaud, O., Dauge, S., Gibot, S., Hraiech, S.,  
971 Jung, B., Kipnis, E., Launey, Y., et al. (2018). Hospital-acquired pneumonia in ICU. Anaesth.  
972 Crit. Care Pain Med.

973 Li, Q., Guan, X., Wu, P., Wang, X., Zhou, L., Tong, Y., Ren, R., Leung, K.S.M., Lau, E.H.Y.,  
974 Wong, J.Y., et al. (2020). Early Transmission Dynamics in Wuhan, China, of Novel  
975 Coronavirus–Infected Pneumonia. *N. Engl. J. Med.* 382, 1199–1207.

976 Lu, R., Zhao, X., Li, J., Niu, P., Yang, B., Wu, H., Wang, W., Song, H., Huang, B., Zhu, N., et  
977 al. (2020). Genomic characterisation and epidemiology of 2019 novel coronavirus:  
978 implications for virus origins and receptor binding. *Lancet* 395, 565–574.

979 De Luca, G., Cavalli, G., Campochiaro, C., Della-Torre, E., Angelillo, P., Tomelleri, A.,  
980 Boffini, N., Tentori, S., Mette, F., Farina, N., et al. (2020). GM-CSF blockade with  
981 mavrilimumab in severe COVID-19 pneumonia and systemic hyperinflammation: a single-  
982 centre, prospective cohort study. *Lancet Rheumatol.* 2, e465–e473.

983 Lucas, C., Wong, P., Klein, J., Castro, T.B.R., Silva, J., Sundaram, M., Ellingson, M.K., Mao,  
984 T., Oh, J.E., Israelow, B., et al. (2020). Longitudinal analyses reveal immunological misfiring  
985 in severe COVID-19. *Nature* 584, 463–469.

986 Mahase, E. (2020). Long covid could be four different syndromes, review suggests. *BMJ*  
987 371, m3981.

988 Mair, F., Hartmann, F.J., Mrdjen, D., Tosevski, V., Krieg, C., and Becher, B. (2016). The end  
989 of gating? An introduction to automated analysis of high dimensional cytometry data. *Eur J*  
990 *Immunol* 46, 34–43.

991 Mathew, D., Giles, J.R., Baxter, A.E., Oldridge, D.A., Greenplate, A.R., Wu, J.E., Alanio, C.,  
992 Kuri-Cervantes, L., Pampena, M.B., D’Andrea, K., et al. (2020). Deep immune profiling of  
993 COVID-19 patients reveals distinct immunotypes with therapeutic implications. *Science* (80-  
994 ). 369, eabc8511.

995 McGough, J.J., and Faraone, S. V (2009). Estimating the size of treatment effects: moving  
996 beyond p values. *Psychiatry (Edgmont)*. 6, 21–29.

997 McInnes, L., Healy, J., Saul, N., and Großberger, L. (2018). UMAP: Uniform Manifold  
998 Approximation and Projection. *J. Open Source Softw.*

999 McInnes L Saul N, Großberger L, H.J. (2018). UMAP: Uniform Manifold Approximation and  
1000 Projection. *JOSS*.

1001 Merad, M., and Martin, J.C. (2020). Pathological inflammation in patients with COVID-19: a  
1002 key role for monocytes and macrophages. *Nat. Rev. Immunol.* 20, 355–362.

1003 Moore, J.B., and June, C.H. (2020). Cytokine release syndrome in severe COVID-19.  
1004 *Science* 368, 473–474.

1005 Nakano, H., Moran, T., Nakano, K., Whitehead, G., Thomas, S., and Cook, D. (2015). CCR2

1006 promotes accumulation of conventional dendritic cells in the lung during inflammation  
1007 (CAM4P.149). *J. Immunol.* *194*, 185.7 LP-185.7.

1008 Nakano, H., Lyons-Cohen, M.R., Whitehead, G.S., Nakano, K., and Cook, D.N. (2017).  
1009 Distinct functions of CXCR4, CCR2, and CX3CR1 direct dendritic cell precursors from the  
1010 bone marrow to the lung. *J. Leukoc. Biol.* *101*, 1143–1153.

1011 Nguyen, A., David, J.K., Maden, S.K., Wood, M.A., Weeder, B.R., Nellore, A., and  
1012 Thompson, R.F. (2020). Human Leukocyte Antigen Susceptibility Map for Severe Acute  
1013 Respiratory Syndrome Coronavirus 2. *J. Virol.* *94*.

1014 O'Driscoll, M., Dos Santos, G.R., Wang, L., Cummings, D.A.T., Azman, A.S., Paireau, J.,  
1015 Fontanet, A., Cauchemez, S., and Salje, H. (2020). Age-specific mortality and immunity  
1016 patterns of SARS-CoV-2. *Nature*.

1017 Pauken, K.E., and Wherry, E.J. (2015). Overcoming T cell exhaustion in infection and  
1018 cancer. *Trends Immunol.* *36*, 265–276.

1019 Pierce, C.A., Preston-Hurlburt, P., Dai, Y., Aschner, C.B., Cheshenko, N., Galen, B.,  
1020 Garforth, S.J., Herrera, N.G., Jangra, R.K., Morano, N.C., et al. (2020). Immune responses  
1021 to SARS-CoV-2 infection in hospitalized pediatric and adult patients. *Sci. Transl. Med.* *12*.

1022 Poland, G.A., Ovsyannikova, I.G., and Kennedy, R.B. (2020). SARS-CoV-2 immunity: review  
1023 and applications to phase 3 vaccine candidates. *Lancet (London, England)* *396*, 1595–1606.

1024 Pontelli, M.C., Castro, I.A., Martins, R.B., Veras, F.P., Serra, L. La, Nascimento, D.C.,  
1025 Cardoso, R.S., Rosales, R., Lima, T.M., Souza, J.P., et al. (2020). Infection of human  
1026 lymphomononuclear cells by SARS-CoV-2. *BioRxiv* 2020.07.28.225912.

1027 Prompetchara, E., Ketloy, C., and Palaga, T. (2020). Immune responses in COVID-19 and  
1028 potential vaccines: Lessons learned from SARS and MERS epidemic. *Asian Pac J Allergy*  
1029 *Immunol.*

1030 R Core, T. (2013). R: A language and environment for statistical computing.

1031 R Studio, T. (2015). RStudio: integrated development for R. RStudio, Inc., Boston, MA URL  
1032 [Http://Www. Rstudio. Com](http://www.rstudio.com) *42*, 84.

1033 Roquilly, A., McWilliam, H.E.G., Jacqueline, C., Tian, Z., Cinotti, R., Rimbert, M., Wakim, L.,  
1034 Caminschi, I., Lahoud, M.H., Belz, G.T., et al. (2017). Local Modulation of Antigen-  
1035 Presenting Cell Development after Resolution of Pneumonia Induces Long-Term  
1036 Susceptibility to Secondary Infections. *Immunity* *47*, 135-147.e5.

1037 Roquilly, A., Torres, A., Villadangos, J.A., Netea, M.G., Dickson, R., Becher, B., and  
1038 Asehnoune, K. (2019). Pathophysiological role of respiratory dysbiosis in hospital-acquired

1039 pneumonia. *Lancet Respir. Med.*

1040 Schulte-Schrepping, J., Reusch, N., Paclik, D., Baßler, K., Schlickeiser, S., Zhang, B.,  
1041 Krämer, B., Krammer, T., Brumhard, S., Bonaguro, L., et al. (2020). Severe COVID-19 Is  
1042 Marked by a Dysregulated Myeloid Cell Compartment. *Cell* 182, 1419-1440.e23.

1043 Silvin, A., Chapuis, N., Dunsmore, G., Goubet, A.-G., Dubuisson, A., Derosa, L., Almire, C.,  
1044 Hénon, C., Kosmider, O., Droin, N., et al. (2020). Elevated Calprotectin and Abnormal  
1045 Myeloid Cell Subsets Discriminate Severe from Mild COVID-19. *Cell* 182, 1401-1418.e18.

1046 Stuart, T., Butler, A., Hoffman, P., Hafemeister, C., Papalexi, E., Mauck, W.M. 3rd, Hao, Y.,  
1047 Stoeckius, M., Smibert, P., and Satija, R. (2019). Comprehensive Integration of Single-Cell  
1048 Data. *Cell* 177, 1888-1902.e21.

1049 Su, Y., Chen, D., Yuan, D., Lausted, C., Choi, J., Dai, C.L., Voillet, V., Duvvuri, V.R.,  
1050 Scherler, K., Troisch, P., et al. (2020). Multi-Omics Resolves a Sharp Disease-State Shift  
1051 between Mild and Moderate COVID-19. *Cell*.

1052 Sullivan, G.M., and Feinn, R. (2012). Using Effect Size-or Why the P Value Is Not Enough. *J.*  
1053 *Grad. Med. Educ.* 4, 279–282.

1054 Szabo, P.A., Dogra, P., Gray, J.I., Wells, S.B., Connors, T.J., Weisberg, S.P., Krupska, I.,  
1055 Matsumoto, R., Poon, M.M.L., Idzikowski, E., et al. (2020). Analysis of respiratory and  
1056 systemic immune responses in COVID-19 reveals mechanisms of disease pathogenesis.  
1057 *MedRxiv Prepr. Serv. Heal. Sci.*

1058 Thwaites, R.S., Sanchez Sevilla Uruchurtu, A., Siggins, M.K., Liew, F., Russell, C.D., Moore,  
1059 S.C., Fairfield, C., Carter, E., Abrams, S., Short, C.-E., et al. (2021). Inflammatory profiles  
1060 across the spectrum of disease reveal a distinct role for GM-CSF in severe COVID-19. *Sci.*  
1061 *Immunol.* 6.

1062 Tian, W., Zhang, N., Jin, R., Feng, Y., Wang, S., Gao, S., Gao, R., Wu, G., Tian, D., Tan,  
1063 W., et al. (2020). Immune suppression in the early stage of COVID-19 disease. *Nat.*  
1064 *Commun.* 11, 5859.

1065 Del Valle, D.M., Kim-Schulze, S., Huang, H.-H., Beckmann, N.D., Nirenberg, S., Wang, B.,  
1066 Lavin, Y., Swartz, T.H., Madduri, D., Stock, A., et al. (2020). An inflammatory cytokine  
1067 signature predicts COVID-19 severity and survival. *Nat. Med.* 26, 1636–1643.

1068 Varga, Z., Flammer, A.J., Steiger, P., Haberecker, M., Andermatt, R., Zinkernagel, A.S.,  
1069 Mehra, M.R., Schuepbach, R.A., Ruschitzka, F., and Moch, H. (2020). Endothelial cell  
1070 infection and endotheliitis in COVID-19. *Lancet (London, England)* 395, 1417–1418.

1071 World Health Organization (2020a). Weekly Epidemiological Update on COVID-19.

1072 World Health Organization (2020b). WHO R&D Blueprint novel Coronavirus COVID-19  
1073 Therapeutic Trial Synopsis. World Heal. Organ. 1–9.

1074 Wrapp, D., Wang, N., Corbett, K.S., Goldsmith, J.A., Hsieh, C.-L., Abiona, O., Graham, B.S.,  
1075 and McLellan, J.S. (2020). Cryo-EM structure of the 2019-nCoV spike in the prefusion  
1076 conformation. *Science* 367, 1260–1263.

1077 Wu, X., Zhang, H., Xing, Q., Cui, J., Li, J., Li, Y., Tan, Y., and Wang, S. (2014). PD-1(+)  
1078 CD8(+) T cells are exhausted in tumours and functional in draining lymph nodes of  
1079 colorectal cancer patients. *Br. J. Cancer* 111, 1391–1399.

1080 Zhang, J.-Y., Wang, X.-M., Xing, X., Xu, Z., Zhang, C., Song, J.-W., Fan, X., Xia, P., Fu, J.-  
1081 L., Wang, S.-Y., et al. (2020a). Single-cell landscape of immunological responses in patients  
1082 with COVID-19. *Nat. Immunol.* 21, 1107–1118.

1083 Zhang, Q., Bastard, P., Liu, Z., Le Pen, J., Moncada-Velez, M., Chen, J., Ogishi, M., Sabli,  
1084 I.K.D., Hodeib, S., Korol, C., et al. (2020b). Inborn errors of type I IFN immunity in patients  
1085 with life-threatening COVID-19. *Science* (80-. ). 370, eabd4570.

1086 Zhao, Y., Kilian, C., Turner, J.-E., Bosurgi, L., Roedl, K., Bartsch, P., Gnirck, A.-C., Cortesi,  
1087 F., Schultheiß, C., Hellmig, M., et al. (2021). Clonal expansion and activation of tissue-  
1088 resident memory-like Th17 cells expressing GM-CSF in the lungs of severe COVID-19  
1089 patients. *Sci. Immunol.* 6.

1090 Zheng, M., Gao, Y., Wang, G., Song, G., Liu, S., Sun, D., Xu, Y., and Tian, Z. (2020).  
1091 Functional exhaustion of antiviral lymphocytes in COVID-19 patients. *Cell. Mol. Immunol.* 17,  
1092 533–535.

1093 Zhou, P., Yang, X.L., Wang, X.G., Hu, B., Zhang, L., Zhang, W., Si, H.R., Zhu, Y., Li, B.,  
1094 Huang, C.L., et al. (2020). A pneumonia outbreak associated with a new coronavirus of  
1095 probable bat origin. *Nature* 579, 270–273.

1096 Zingaropoli, M.A., Perri, V., Pasculli, P., Cogliati Dezza, F., Nijhawan, P., Savelloni, G., La  
1097 Torre, G., D’Agostino, C., Mengoni, F., Lichtner, M., et al. (2020). Major reduction of NKT  
1098 cells in patients with severe COVID-19 pneumonia. *Clin. Immunol.* 222, 108630.

1099

# Figure 1

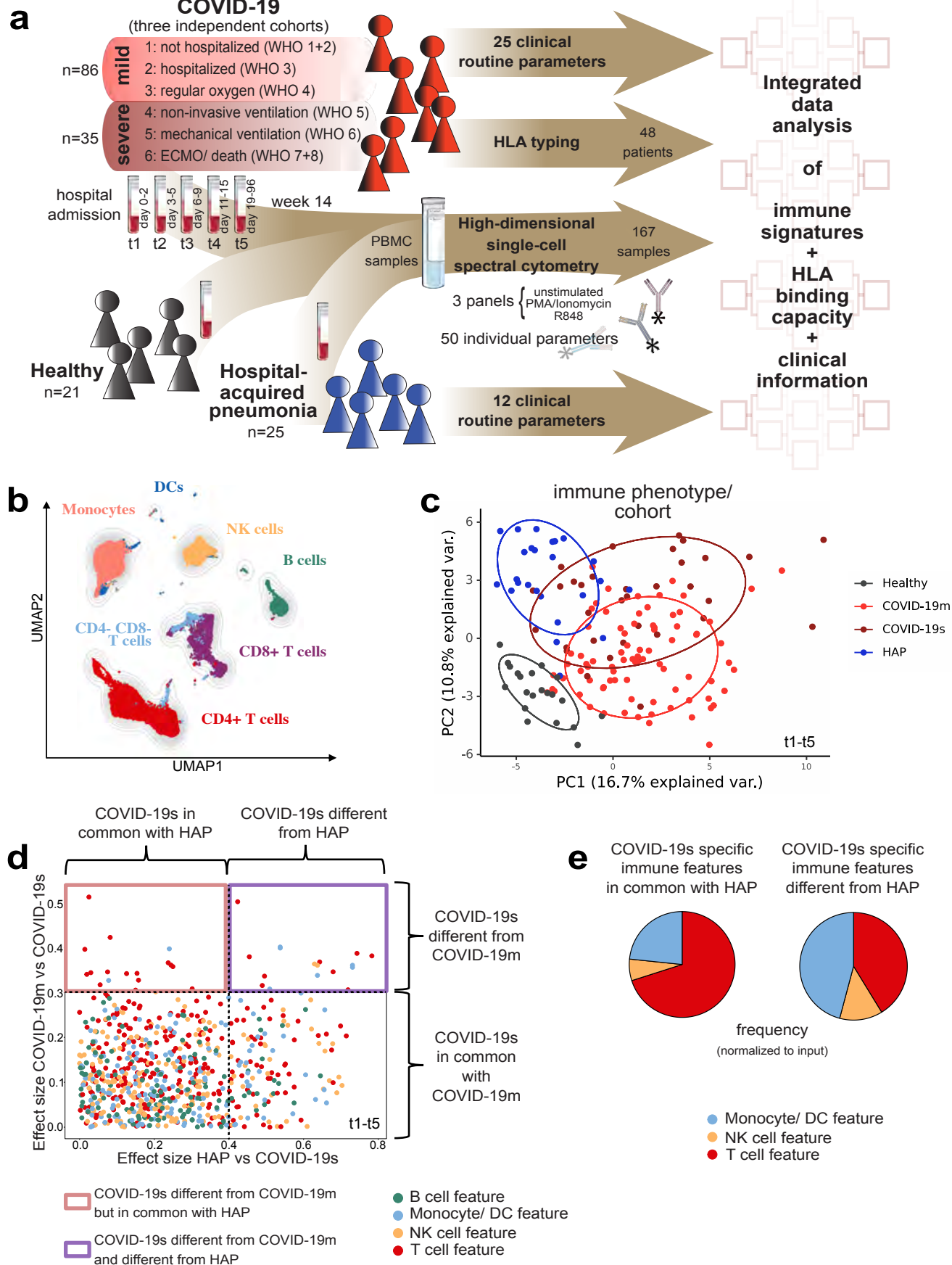


# Figure 2

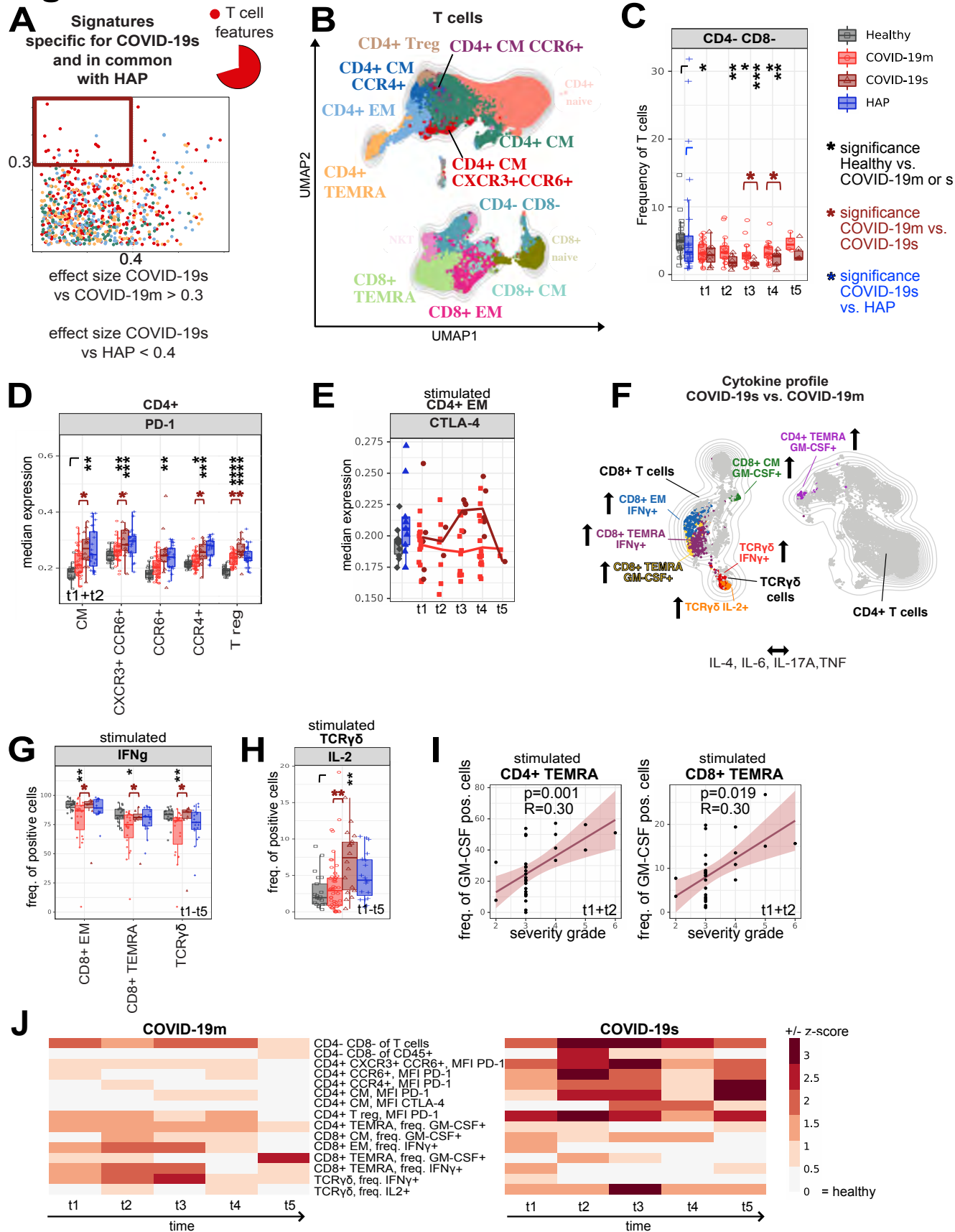


# Figure 3

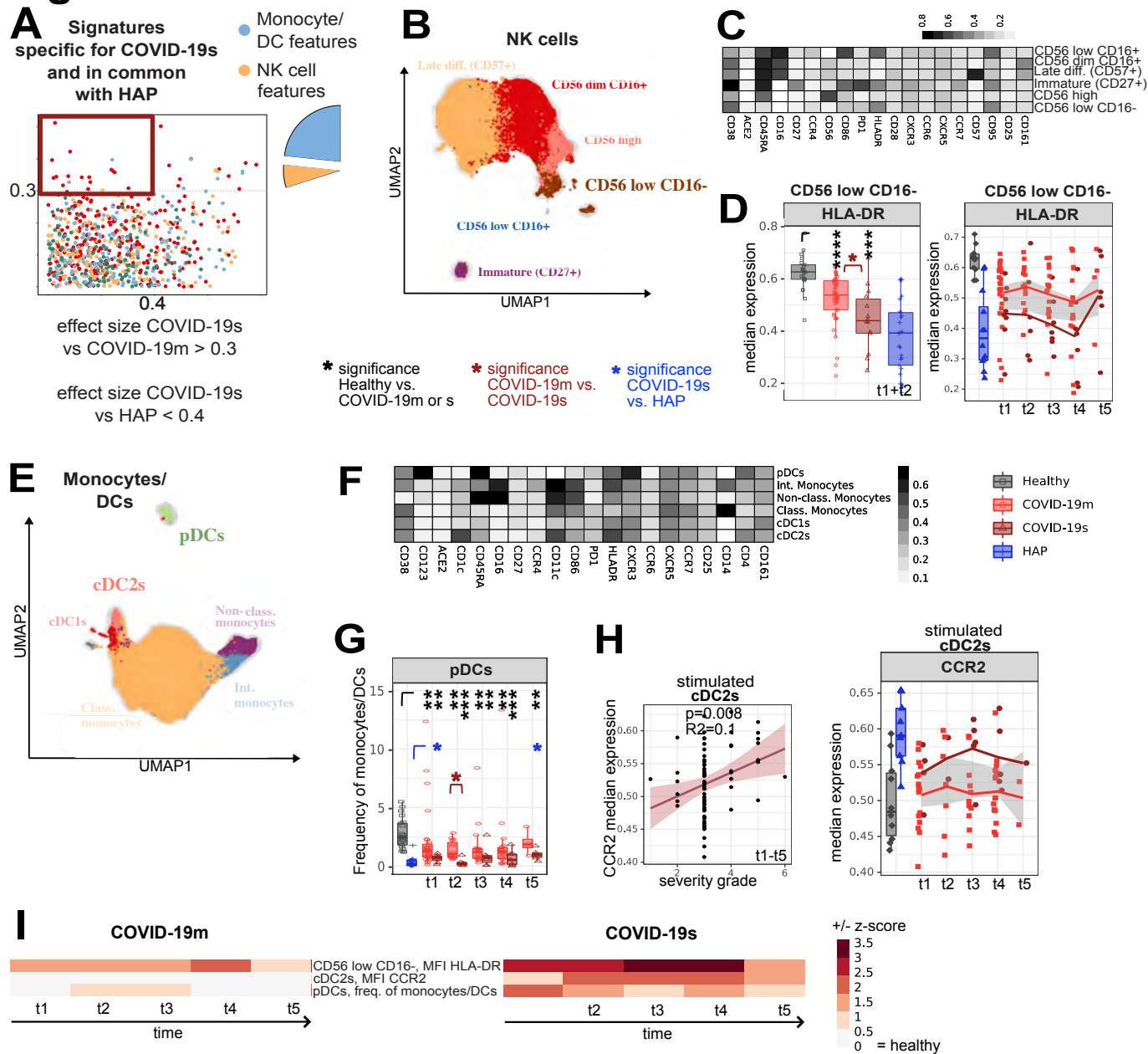
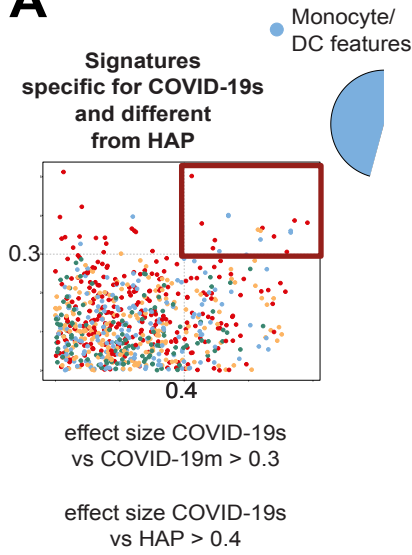
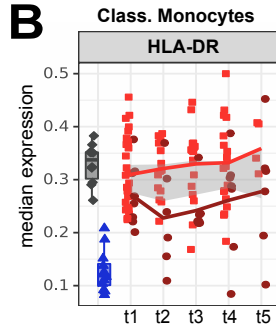


# Figure 4

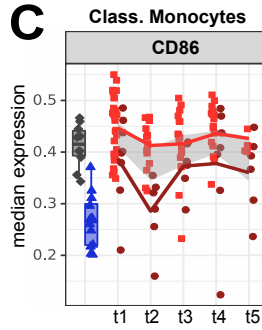
**A**



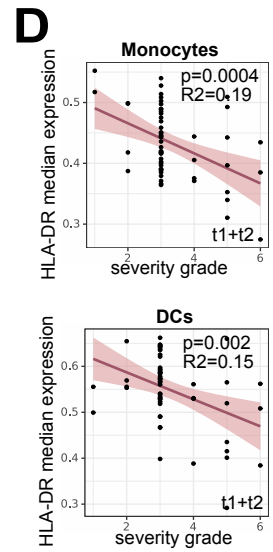
**B**



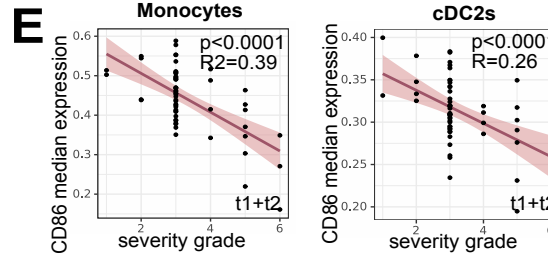
**C**



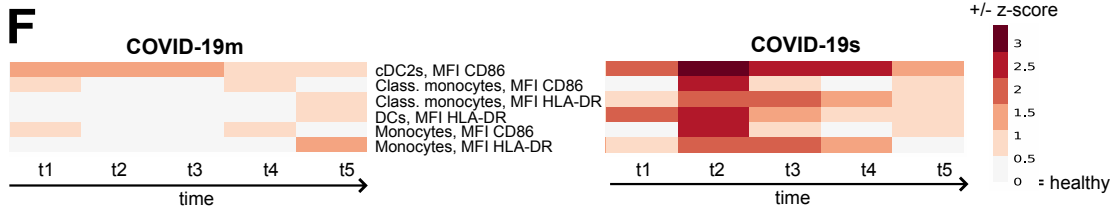
**D**



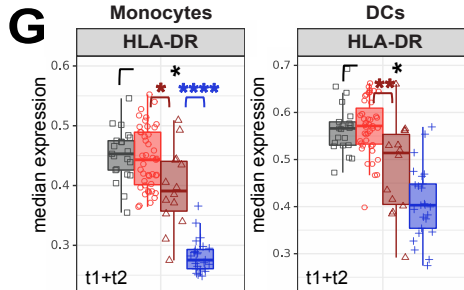
**E**



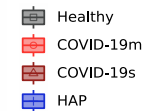
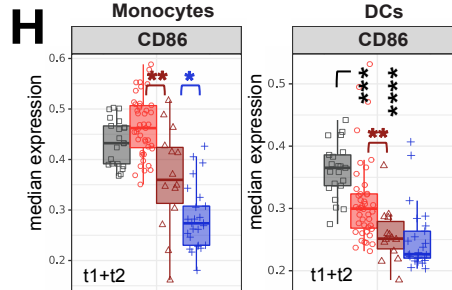
**F**



**G**



**H**



- \* significance Healthy vs. COVID-19m or s
- \* significance COVID-19m vs. COVID-19s
- \* significance COVID-19s vs. HAP

# Figure 5

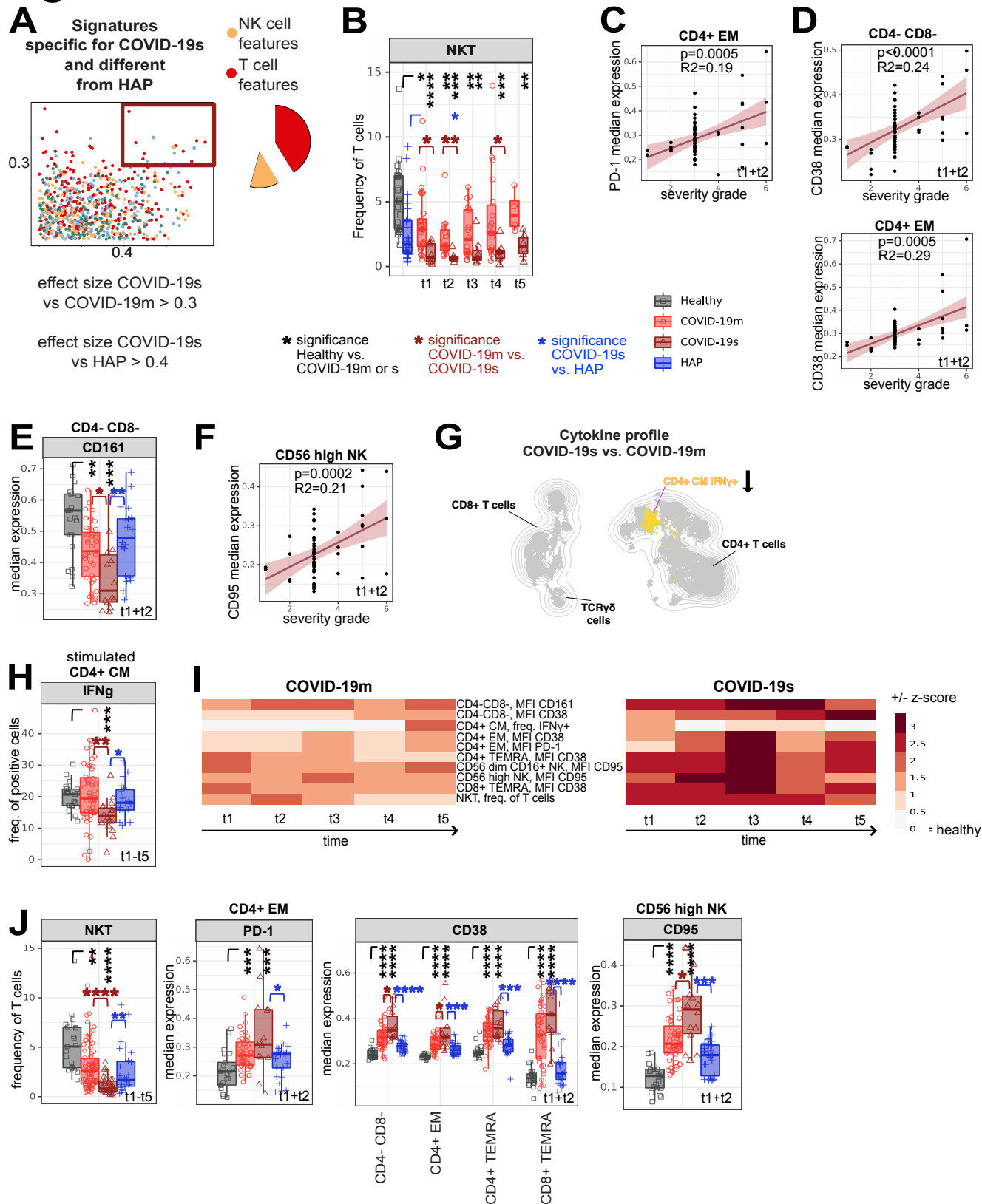
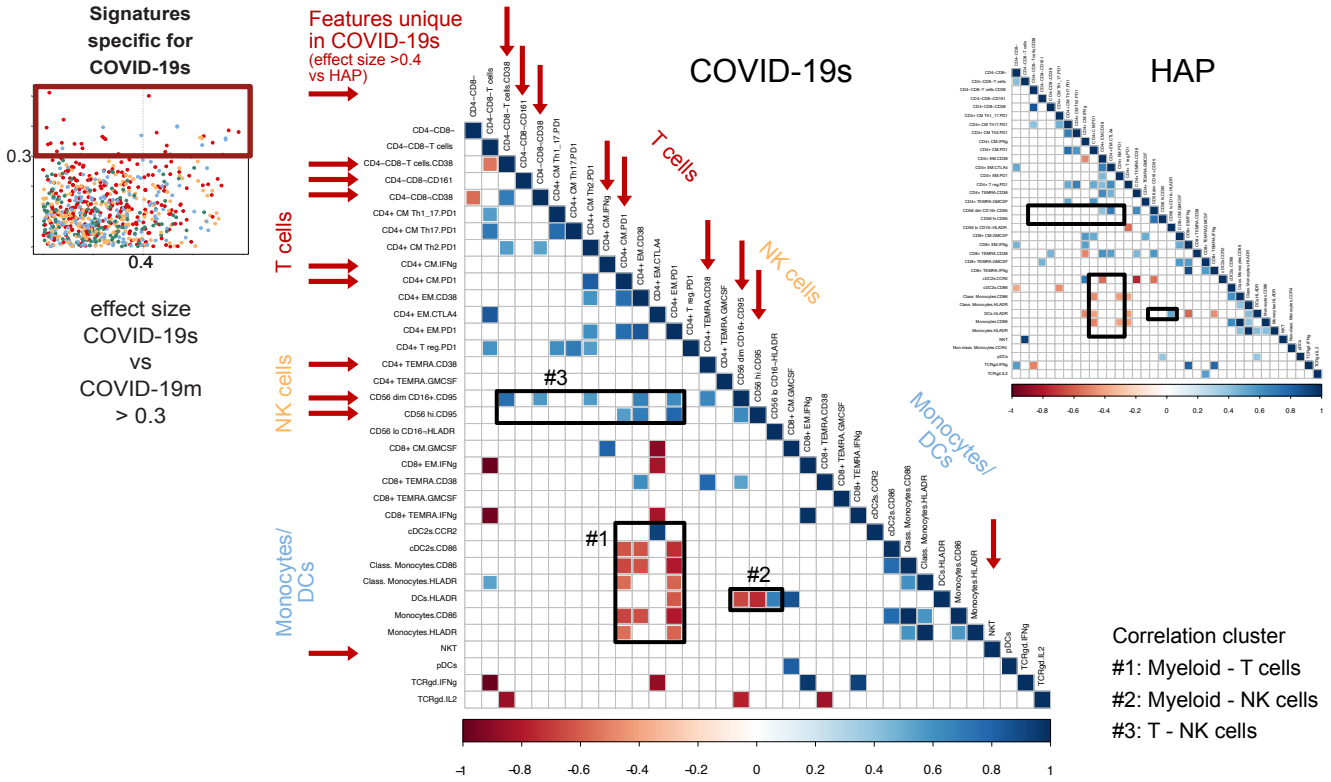
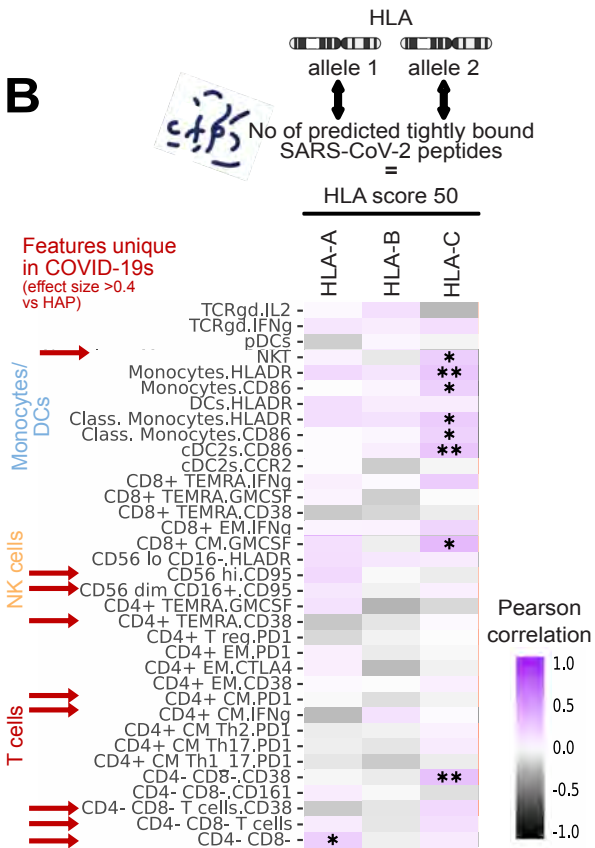


# Figure 6

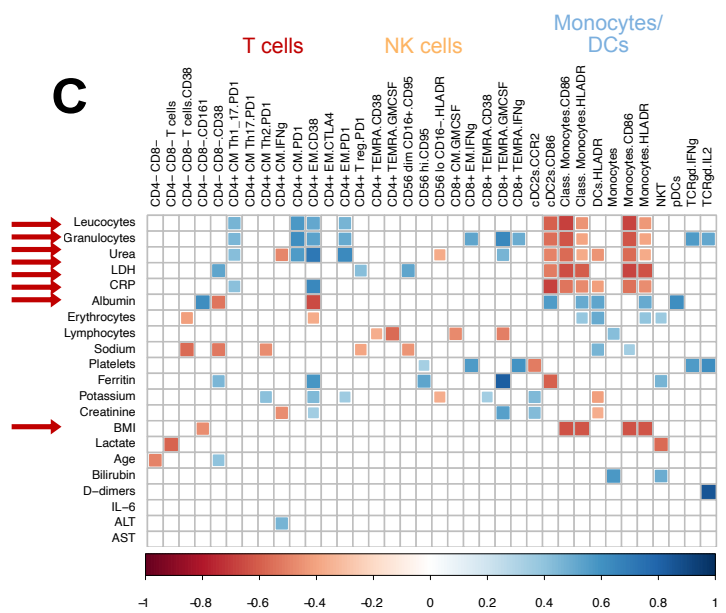
## A



## B



## C



## D

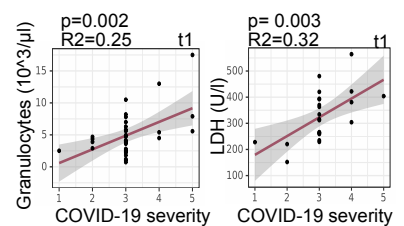


# Figure 7

